Atmospheric
Chemistry
and Physics
Discussions

1 **Wintertime organic and inorganic aerosols in Lanzhou, China:**

2 **Sources, processes and comparison with the results during**

3 **summer**

4

5 **J. Xu[1], J. Shi[2], Q. Zhang[3], X. Ge[4], F. Canonaco[5], A. S. H. Prévôt[5, 6], M. Vonwiller[7], S.**

6 **Szidat[7], J. Ge[2], J. Ma[8], Y. An[1], S. Kang[1], D. Qin[1]**

7 [1]State Key Laboratory of Cryospheric Sciences, Cold and Arid Regions Environmental

8 and Engineering Research Institute, CAS, Lanzhou 730000, China

9 [2]Key Laboratory for Semi-Arid Climate Change of the Ministry of Education, College of

10 Atmospheric Sciences, Lanzhou University, Lanzhou 730000, China

11 [3]Department of Environmental Toxicology, University of California, Davis, CA 95616,

12 USA

13 [4]Jiangsu Key Laboratory of Atmospheric Environment Monitoring and Pollution Control

14 (AEMPC), School of Environmental Science and Engineering, Nanjing University of

15 Information Science & Technology, Nanjing 210044, China

16 [5]Laboratory of Atmospheric Chemistry, Paul Scherrer Institute (PSI), Villigen 5232,

17 Switzerland

18 [6]State Key Laboratory of Loess and Quaternary Geology and Key Laboratory of Aerosol

19 Chemistry and Physics, Institute of Earth Environment, Chinese Academy of Sciences,

20 710075 Xi'an, China

21 [7]Department of Chemistry and Biochemistry & Oeschger Centre for Climate Change

22 Research, University of Bern, Berne, 3012, Switzerland

23 [8]College of Earth Environmental Science, Lanzhou University, Lanzhou 730000, China

24

25 Correspondence to: J. Xu (jzxu@lzb.ac.cn)

Atmospheric
Chemistry
and Physics
Discussions

26

Abstract

28　Lanzhou, which is located in a steep Alpine valley in western China, is one of the most

29　polluted cities in China during the wintertime. In this study, an Aerodyne high resolution

30　time-of-flight aerosol mass spectrometer (HR-ToF-AMS), a seven-wavelength

31　aethalometer, and a scanning mobility particle sizer (SMPS) were deployed during

32　January 10 to February 4, 2014 to study the mass concentrations, chemical processes, and

33　sources of sub-micrometer particulate matter (PM_1). The average PM_1 concentration

34　during this study was 57.3 μg m^{-3} (ranging from 2.1 to 229.7 μg m^{-3} for hourly averages)

35　with organic aerosol (OA) accounting for 51.2%, followed by nitrate (16.5%), sulphate

36　(12.5%), ammonium (10.3%), black carbon (BC, 6.4%), and chloride (3.0%). The mass

37　concentration of PM_1 during winter was more than twice the average value observed at

38　the same site in summer 2012 (24.5 μg m^{-3}), but the mass fraction of OA was similar in

39　the two seasons. Nitrate contributed a significantly higher fraction to the PM_1 mass in

40　winter compared to summer, largely due to more favoured partitioning to the particle

41　phase at low air temperature. The mass fractions of both OA and nitrate increased by ~5%

42　with the increase of the total PM_1 mass loading, while the average sulphate fraction

43　decreased by 6%, indicating the importance of OA and nitrate for the heavy air pollution

44　events in Lanzhou. The size distributions of OA, nitrate, sulphate, ammonium, and

45　chloride all peaked at ~500 nm with OA being slightly broader, suggesting that aerosol

46　particles were externally mixed during winter, likely due to stagnant air conditions

47　(average wind speed: 0.82 m s^{-1}). All species showed evident diurnal variations reflecting

48　the important local/regional sources.

49

50　The average mass spectrum of OA showed a medium oxidation degree (average O/C

51　ratio of 0.28), which was lower than that during summer 2012. This is consistent with

52　weaker photochemical processing during winter. Positive matrix factorization (PMF)

53　with the multi-linear engine (ME-2) solver identified six OA sources, i.e., a hydrocarbon-

54　like OA (HOA), a biomass burning OA (BBOA), a cooking-emitted OA (COA), a coal

Atmospheric
Chemistry
and Physics
Discussions

55   combustion OA (CCOA), and two oxygenated OA (OOA) factors. One of the OOAs was

56   semi-volatile (SV-OOA) and the other one of low-volatility (LV-OOA). SV-OOA was

57   the most abundant OA component (24% of OA mass), followed by COA (20%), LV-

58   OOA (19%), CCOA (18%), BBOA (11%), and HOA (9%). The mass fraction of primary

59   OA (= HOA + BBOA + COA + CCOA) increased during high PM pollution periods,

60   indicating that local primary emissions were a main reason for the formation of haze in

61   Lanzhou during winter. The primary OA sources were more complex during winter than

62   during summer. Radiocarbon (^{14}C) measurement was conducted on four $PM_{2.5}$ filter

63   samples from this study, which allowed for a quantitative source apportionment of

64   organic carbon (OC). The non-fossil sources on average accounted for $55 \pm 3\%$ of OC

65   which could be mainly from biomass burning and cooking activities, suggesting the

66   importance of non-fossil sources for the PM pollution in Lanzhou. Combining with the

67   PMF results, we also found that a large fraction (57%) of the secondary OC was from

68   non-fossil OC.

69

70   **1   Introduction**

71   Frequent haze pollution events in urban areas in China have been a widespread concern

72   in recent years due to its high adverse health effects, visibility degradation and climate

73   effects (Chan and Yao, 2008). The Chinese Central Government had put in extensive

74   efforts to find urgent and suitable control strategies to reduce further deterioration of air

75   quality. Strategies such as promoting energy conservation and emission reduction

76   measures and new air quality standards ($PM_{2.5}$ currently *vs*. PM_{10} in the past) have been

77   implemented in the last three years. Many local governments have also launched

78   measures such as shutting down some highly polluting factories and restricting the use of

79   private vehicles to reduce air pollution in their cities. However, air pollution in China is

80   still far from being controlled due to its complex sources and limited knowledge on the

81   multiple pathways leading to secondary aerosol formation and dynamic variation of

82   aerosol mass loading.

83

Atmospheric
Chemistry
and Physics
Discussions

84 Lanzhou, the capital of Gansu province, is located at the northwest of China and has
85 experienced air pollution issues since the 1960s due to emissions from the petrochemical
86 industry and its valley terrain. Air pollution is still serious and has become more variable
87 in recent years (since 2000) because of fast urbanization and increased energy
88 consumption. The severity of air pollution often reaches maximum intensity during
89 winter due to coal combustion for domestic heating and cooking, similar to the situations
90 in most cities of northern China (Wang et al., 2014); In addition, the stagnant
91 meteorological conditions during winter in Lanzhou such as calm wind and shallow
92 planetary boundary layer (PBL) caused by its valley terrain, are also important factors
93 influencing the transport and diffusion of air pollutants. Despite the serious air pollution
94 during winter in Lanzhou, aerosol chemistry, sources, and formation and transformation
95 processes were poorly documented in the literature, which limit the development and
96 implementation of efficient control strategies.

97

98 The chemical and physical properties of atmospheric aerosol particles during winter,
99 especially during haze episode, have been investigated in metropolitan cities in Eastern
100 China (Sun et al., 2006; Zhao et al., 2013; Huang et al., 2014; Sun et al., 2014). For
101 example, the mean aerosol optical depth at 500 nm were up to ~0.7 during the month-
102 long heavy haze pollution episode during January 2013 in Beijing (Bi et al., 2014); The
103 airborne microbes were found in particulate matter (PM) during hazy period which may
104 potentially include respiratory microbial allergens and pathogens (Cao et al., 2014).
105 Collection and analysis of filter samples have enabled quantification of the chemical
106 composition of PM using a suite of off-line instruments (such as ion chromatography,
107 organic and element carbon analyzer, inductively coupled plasma-mass spectrometry and
108 so on) in the laboratory (He et al., 2001; Zheng et al., 2005; Sun et al., 2006; Sun et al.,
109 2011a; Zhang et al., 2013; Zhao et al., 2013). Semi-continuous measurement with hourly
110 time resolution on chemical composition of aerosol particle is better compared to filter
111 collection for elucidating the chemical processes during haze episodes (Gao et al., 2011;
112 Xue et al., 2014; Zheng et al., 2015).

Atmospheric
Chemistry
and Physics
Discussions

Open Access

EGU

113

114   Previous studies on source apportionment of aerosol particle identified dust, traffic,

115   industry, cooking-related activities, and secondary formation as important contributors,

116   although the contributions of individual sources may change drastically with location,

117   season, and different apportionment algorithms (Zheng et al., 2005; Yu et al., 2013;

118   Huang et al., 2014). For example, Zheng et al. (2005) used chemical mass balance

119   (CMB) to quantitatively apportion the sources that contribute to fine PM concentration in

120   Beijing and found coal combustion contributed 16% of fine PM mass in January. By

121   contrast, principal component analysis of the same dataset estimated almost twice amount

122   of aerosols from coal combustion (Song et al., 2006). Source apportionment techniques -

123   such as positive matrix factorization (PMF) allow for using thousands of individual

124   species for source identification and the error of analysis to constrain the fitting, and

125   would thus appear more suitable to identify and apportion PM to their sources. Compared

126   with the number of aerosol source apportionment studies using PMF in Eastern China

127   (e.g., Sun et al., 2013b; Zhang et al., 2013), there were fewer studies in inland cities of

128   China (Elser et al., 2016), the results of which can be used for inter-comparison and

129   understanding the difference of aerosol pollution in different parts of China. In addition,

130   it has been known that a large mass fraction of ambient PM during haze episodes is from

131   fine particles, of which secondary species (some carbonaceous components, sulphate,

132   nitrate, and ammonium) are major components (Zhao et al., 2013). However, the

133   formation and evolution mechanisms of those secondary species were relatively poorly

134   understood (Sun et al., 2014). The possible fast chemical reactions occurring during haze

135   pollution further complicate our understanding of the formation processes of secondary

136   aerosol, where high time resolution instruments are likely the best tools to be used.

137

138   Online instruments based on mass spectrometric techniques, such as Aerodyne aerosol

139   mass spectrometer (AMS) (Jayne et al., 2000), appear to be the most advanced on

140   probing the fast aerosol chemical processes because of the output of a large amount of

141   chemical information and its fine time resolution (in minutes) and mass sensitivity (in ng

Atmospheric
Chemistry
and Physics
Discussions

142   m^{-3}) (Canagaratna et al., 2007). Aerodyne high resolution time-of-flight mass

143   spectrometer (HR-ToF-AMS) have been widely employed for the chemical

144   characterization of submicron aerosol (PM$_1$) (DeCarlo et al., 2006). The instrument

145   provides on-line quantitative mass spectra of the non-refractory (inorganic and organic)

146   aerosol components with high time resolution. Frequently, the organic aerosol (OA) can

147   be further analyzed using the PMF algorithm (Ulbrich et al., 2009; Zhang et al., 2011b),

148   which can represent the organic mass spectral matrix as a set of source/process-related

149   factor mass spectra and time series. In addition, carbon isotope technique has been

150   recently applied to quantify the fossil/non-fossil origins of carbonaceous aerosols, and in

151   combination with AMS-PMF analyses, the assessment of the origin of secondary organic

152   aerosol (SOA) became possible (Minguillon et al., 2011; Huang et al., 2014; Zotter et al.,

153   2014; Beekmann et al., 2015).

154

155   In a previous study, we used an HR-ToF-AMS, to investigate the chemical characteristics

156   PM$_1$ in the urban area of Lanzhou during summer 2012 (Xu et al., 2014). During that

157   study, organics in PM$_1$ was found to mainly originate from traffic, cooking activities, and

158   chemical reactions which produced semi-volatile and less-volatility oxygenated OA.

159   Compared to summer situation, energy consumption for heating is huge during winter

160   and the dry and stable meteorological condition in the basin leads to longer aerosol

161   lifetime during winter. Thus aerosols are influenced largely by very different chemical

162   processes between the two seasons. Thus, more intensive measurements of PM chemical

163   characteristics are needed to better understand aerosol sources, to quantify their lifetime

164   in the atmosphere and to constrain the uncertainties of their climatic influences. During

165   winter of 2013/2014, we conducted such a study at an urban site of Lanzhou. In this

166   paper, we focus on the chemical speciation of PM$_1$ and source apportionment of OA.

167

168   2   Measurement and methods

169   2.1   Sampling site

170   Aerosol particle measurements were conducted from January 10 to February 4, 2014, at

171   the top floor of a twenty-two story building (~70 m a.g.l) (36.05 °N; 103.85 °W, 1569 m

172   a.s.l) in the campus of Lanzhou University (Fig. S1a). The campus is located in the

173   Chenguan district of Lanzhou which is a cultural and educational area. The twenty-two

174   story building sits at the western edge of the campus and faces a south-northern arterial

175   road (Fig. S1a). At the campus side of this building, there is a three story dining hall of

176   Lanzhou University, and over the arterial road side, there are many restaurants and

177   residents. The room temperature was kept at ~20 ℃ by a central heating radiator. The

178   weather in Lanzhou during the campaign was cold (avg. T = 0.5 ℃) and dry (avg. RH =

179   28%), and was influenced by the Asian winter monsoon. Because Lanzhou is surrounded

180   by mountains, atmospheric condition is normally stable with low wind speed (0.82 m s^{-1}

181   during this study). The sampling site represents a typical urban area dominated by

182   residential and commercial area.

183

184   2.2   Instruments

185   The physiochemical properties of aerosol particles were monitored in real-time by a suite

186   of instruments (Fig. S1b). The sampling inlet, constructed using 0.5 inch copper tube,

187   stemmed out of the rooftop by about 1.5 m. A PM$_{2.5}$ cyclone (model URG-2000-30EH,

188   URG Corp., Chapel Hill, NC, USA) was used for removing coarse particles. The length

189   of the sampling line was about 5 m. A diffusion dryer was placed upstream of this line to

190   eliminate potential relative humidity (RH) effect on particles. The inlet was shared by an

191   Aerodyne HR-ToF-AMS (Aerodyne, Inc., Billerica, MA, USA) for the size-resolved

192   chemical speciation of non-refractory sub-micrometer PM (NR-PM$_1$), a single particle

193   intra-cavity laser induced incandescence photometer (SP2, DMT, Inc., Boulder, CO,

194   USA) for   refractory black carbon (rBC) measurement, a customer-made scanning

195   mobility particle sizer (SMPS) (Wiedensohler et al., 2012) for measuring particle size

196   distribution between 10-800 nm, and a 7-λ aethalometer (model AE31, Magee Scientific,

Atmospheric
Chemistry
and Physics

Discussions

197   Berkeley, CA, USA) to derive the mass concentration of light absorbing black carbon

198   (BC) particles. The total air flow rate from the inlet was ~ 16 L min^{-1}, with a vacuum

199   pump drawing the air at a flow rate of 10 L min^{-1} and the other 6 L min^{-1} sampled by the

200   instrument. The retention time of particles in the sampling line was less than 2.5 s. A

201   parallel inlet with a 1:10 dilution stage was setup for real-time PM$_{2.5}$ measurement using

202   a tapered element oscillating microbalance (TEOM series 1400a, R&P, East Greenbush,

203   NY, USA). The roof of the building also hosted instruments for monitoring

204   meteorological parameters such as visibility, air temperature, wind direction, wind speed,

205   and RH. The visibility was measured with a LED-based (880 nm) forward (42 °)

206   scattering visibility sensor (model M6000, Belfort Ins., Maryland, USA).

207

208   2.2.1   HR-ToF-AMS operation

209   A detailed description of the principle and design of HR-ToF-AMS can be found

210   elsewhere (Jayne et al., 2000; DeCarlo et al., 2006). Briefly, HR-ToF-AMS consists of

211   three major sections: the inlet system, the particle sizing vacuum chamber, and the

212   particle composition detection section. The combination of a 100 μm orifice and an

213   aerodynamic lens in the inlet system are used to focus the airborne particles into a

214   concentrated and narrow beam, and then accelerated into the vacuum chamber (~10^5

215   Torr) modulated by a chopper for measuring aerodynamic size of the particle; Before

216   being detected, the particles are flash vaporized under 600 °C and ionized by a 70 eV

217   electron impact, and finally detected by the high resolution time-of-flight mass

218   spectrometer. The chopper works at three positions alternately, i.e., an open position

219   which transmits the particle beam continuously, a close position which blocks the particle

220   beam completely, and a chopping position which modulates the beam transmission (2%

221   duty cycle). The open and close positions yield the bulk and background signals for the

222   airborne particle, respectively, while the chopping position modulates the particle beam

223   by spinning chopper wheel (~150 Hz) to yield size-resolved spectral signals. The mass

224   spectrometer in the detection section works in two modes based on the ionic path, i.e., V-

225   mode and W-mode, with high sensitivity and high chemical resolution (~6000 m/Δm),

Atmospheric
Chemistry
and Physics
Discussions

226 respectively. The highly sensitive V-mode signals are usually used for reporting mass

227 concentration, while the high chemical resolution W-mode signals are used for the

228 analyses of mass spectrum. The time resolution for both V and W modes was 5 min.

229 Under V-mode, the instrument switched between the mass spectrum mode and the PToF

230 mode every 15 s, spending 6 and 9 s on each, and cycled 20 times in one run; No PToF

231 data were recorded in W-mode due to low signal-to-noise (S/N) ratios.

232

233 The instrument was calibrated for ionization efficiency (IE), inlet flow rate, and particle

234 sizes using the standard procedure described by (Jayne et al., 2000). These three

235 calibrations were performed at the beginning, in the middle and end of the field study.

236 Particle-free ambient air was sampled at the end of the study to determine the detection

237 limits (DLs) of individual species and also for adjusting the fragmentation table. Default

238 relative ionization efficiency (RIE) values were assumed for organics (1.4), nitrate (1.1),

239 sulphate (1.2), and chloride (1.3), while an RIE value of 3.9 was determined for

240 ammonium following the analysis of pure NH_4NO_3. The close concentrations between

241 measured ammonium and predicted ammonium based on the stoichiometric charge

242 balance between nitrate, sulphate, and chloride (slope = 0.94, Fig. S4) suggest that these

243 RIE values are suitable for this campaign.

244

245 2.2.2   Operations of other instruments

246 The SMPS consisted of a condensation particle counter (CPC) (TSI, model 3772) and a

247 differential mobility analyser (DMA) was deployed at 5 min interval. Sample and sheath

248 flow rates of the DMA were set to 1 L min^{-1} and 5 L min^{-1}, respectively. The SMPS was

249 calibrated using a polystyrene latex (PSL) standard prior to field measurements.

250

251 The SP2 uses an intra-cavity Nd:YAG laser at 1064 nm to determine the optical size of a

252 single particle by light scattering and, if material within the particle absorbs at this laser

253 wavelength, the refractory mass of the particle quantified by detection of the main light-

Atmospheric
Chemistry
and Physics
Discussions

254   absorbing component is rBC. The SP2 incandescence signal was used to obtain single

255   particle rBC mass after calibration with Aquadag standard BC particles. The measured

256   rBC mass is converted to a mass equivalent diameter, which is termed as the BC core

257   diameter (D_c) - the diameter of a sphere containing the same mass of rBC as measured in

258   the particle. Any measured particle with a detectable incandescence signal is referred to

259   as an rBC particle, whereas a particle which only exhibits a scattering signal is termed as

260   a non-BC particle. The total rBC mass loading is reported as the sum of all detected

261   single particle rBC masses.

262

263   The aethalometer measures the optical attenuation (absorbance) of light from LED lamps

264   emitting at seven wavelengths (370, 470, 520, 590, 660, 880, and 950 nm) with a typical

265   half-width of 20 nm. The difference in light transmission through the particle-laden

266   sample spot and a particle free reference spot of the filter is attributed to the absorption

267   caused by aerosol. The attenuation of light is converted to the BC mass concentration

268   using wavelength-dependent calibration factors as recommended by the manufacturer.

269   BC was measured using data at 880 nm using a specific attenuation cross section of 16.6

270   m^2 g^{-1} and an empirical correction factor (2.14) for the shadowing effect during the

271   campaign. The flow rate was maintained at 4.8 L min^{-1} calibrated using a flow meter.

272   Detection limit of the aethalometer BC was determined to be 0.16–0.28 µg m^{-3} with a

273   flow rate of 4.8 LPM and 5 min time interval, calculated as three times the standard

274   deviation (3σ) of the dynamic blanks. The TEOM was operated at a temperature of 40 °C

275   in order to minimize mass loss due to volatilization of semi-volatile aerosol compounds.

276   The time resolution of $PM_{2.5}$ mass concentration was 5 min.

277

278   2.3   Data processing

279   2.3.1   General AMS data processing

280   The HR-ToF-AMS data were processed using the standard software of SQUIRREL

281   (v1.56)   and   PIKA   (v1.15c)   (http://cires.colorado.edu/jimenez-

282   group/ToFAMSResources/ToFSoftware/index.html)   to   determine   the   mass

Atmospheric
Chemistry
and Physics
Discussions

Open Access

283   concentrations and the size distributions of the NR-PM$_1$ species and the ion-speciated

284   mass spectra of organics, written in IGOR (Wavemetrics, Inc., Lake Oswego, OR, USA).

285   An empirical particle collection efficiency (CE) of 0.5 was used, which has been widely

286   used in field studies employing AMS with a dryer installed in front of the equipment's

287   particle inlet. This CE value was further validated by the consistency between HR-ToF-

288   AMS and SMPS data ($R^2 = 0.9$, Slope = 1.48, Fig. 3). The elemental ratios of OA (O:C,

289   H:C, and OM:OC) for this study was determined using the "Aiken ambient" method

290   (Aiken et al., 2008) other than the "improved-ambient" method (Canagaratna et al., 2015)

291   which increased O:C on average by 27%, H:C on average by 10%, and OM:OC on

292   average by 7% (Fig. S2). These "Aiken ambient" results of elemental ratios are more

293   suitable here to allow for comparison with those during summer 2012.

294

295   2.3.2   Positive Matrix Factorization (PMF) analyses

296   The source decomposition of organics was analysed by PMF with the multilinear engine

297   (ME-2) algorithm which serves to reduce rotational ambiguity within the PMF2

298   algorithm. The ME-2 algorithm allows the user to add a priori information into the model

299   (e.g., source profiles) to constrain the matrix rotation and separate the mixed solution or

300   the weak solution. The PMF analysis of organic matrix using ME-2 algorithm is

301   implemented within the toolkit SoFi (Source Finder) and perform by the so-called a-value

302   approach (Canonaco et al., 2013). First, organic matrix was analysed using the PMF2.exe

303   algorithm in robust mode (Paatero and Tapper, 1994) and explored using the PMF

304   Evaluation Toolkit (PET) (Ulbrich et al., 2009). The PMF solution was evaluated

305   following the procedures outlined in Table 1 of Zhang et al. (2011a) including

306   modification of the error matrix and downweight of low S/N ions. Moreover, based on

307   the AMS fragmentation table, some organic ions were not directly measured but scaled to

308   the organic signal at m/z 44, which were downweighted by increasing their errors by a

309   factor of 3. Some highly polluted periods were deleted during PMF analysis such as

310   January 22-23, 2014. The results of four, five, and six factor solutions with ƒPeak at 0 are

311   shown in supplementary material (Fig. S5-S7). It is easy to find that a hydrocarbon-like

Atmospheric
Chemistry
and Physics
Discussions

312   OA (HOA) factor, a cooking-emitted OA (COA) factor, a semi-volatile and low-volatility

313   oxygenated OA (SV-OOA and LV-OOA) factors could be clearly separated in the four-

314   factor solution; for the HOA factor, there were significant contributions from m/z 60, 73,

315   92, and 115 in the mass spectrum, suggesting a mixing of multiple sources. In the five-

316   factor solution, a coal combustion-emitted OA (CCOA) factor was separated; however,

317   m/z 60 and 73 which are related to biomass burning OA (BBOA) could not be separated.

318   We then performed OA source apportionment using the ME-2 algorithm by constraining

319   the profiles of HOA and BBOA with the fixed a-value of 0.1 for HOA and 0.4 for BBOA.

320   The a-value test was performed following the technical guidelines presented in Crippa et

321   al. (2014). The reference profile of HOA was adopted from the HOA of the summer

322   study and the reference profile of BBOA was adopted from the nine-factor PMF solution

323   of this study.

324

325   The size distributions of individual OA factors were determined via a multivariate linear

326   regression technique (Ge et al., 2012). This algorithm assumes that each OA mass

327   spectrum is the linear superposition of the mass spectra of individual OA factors, whose

328   mass profiles are constant across the whole size range. Further details about the algorithm

329   can be found in Xu et al. (2014).

330

331   2.3.3   Radiocarbon (^{14}C) data analysis

332   In order to identify the origins of SOA, we conducted ^{14}C analysis on four filter samples.

333   These filter samples were collected at the CAEERI site which is about 500 m away from

334   the LZU site (Fig. S1a). Filter samples were collected using a low volume $PM_{2.5}$ sampler

335   (16.7 L min^{-1}) during January 2014 with a 24 h sampling time in every week for each

336   filter (January 3rd, 8th, 15th, and 23rd, respectively) on pre-baked quartz filters. One

337   field blank filter was collected and analysed to correct the filter sample measurements.

338   Organic carbon (OC) was separated from the filters by combustion at 375 ℃ during 200

339   s in pure oxygen in a thermo-optical OC/EC analyser (Model 4L, Sunset Laboratory Inc,

340   USA) (Zhang et al., 2012). The carbon isotopic analysis was conducted by online

Atmospheric
Chemistry
and Physics
Discussions

341   coupling of the OC/EC analyser with the accelerator mass spectrometry system

342   MICADAS at the University of Bern, Switzerland (Zotter et al., 2014; Agrios et al.,

343   2015). Fossil ^{14}C measurement results were transferred into the non-fossil fraction (f_{NF})

344   of OC using a conversion factor of 1.03.

345

346   For the apportionment of AMS-PMF OA factors using ^{14}C data (Zotter et al., 2014), we

347   assume that all OC sources are represented by the six PMF factors and the f_{NF} in NR-PM$_1$

348   was the same as that in PM$_{2.5}$. The OA mass of each PMF factor and total OA were first

349   converted to OC mass using the OM:OC ratios derived from its MS (OM:OC$_{HOA}$ = 1.29,

350   OM:OC$_{BBOA}$ = 1.5, OM:OC$_{COA}$ = 1.27, OM:OC$_{CCOA}$ = 1.37, OM:OC$_{SV-OOA}$ = 1.55,

351   OM:OC$_{LV-OOA}$ = 2.01, OM:OC$_{total}$ = 1.51). For the OC mass concentration of the AMS

352   factors, the following notations, hydrocarbon-like organic carbon (HOC), biomass

353   burning organic carbon (BBOC), cooking organic carbon (COC), coal combustion

354   organic carbon (CCOC), oxygenated organic carbon (OOC), total organic carbon from

355   AMS (TOC$_{AMS}$), were adopted in the following sections. An f_{NF} value was assumed a

356   priori for the primary PMF factors HOC, BBOC, COC, and CCOC. The average f_{NF} of

357   OOC is then derived by the equation below:

358

359    $f_{NF\_OOC} = (TOC_{NF\_AMS} - f_{NF\_HOC} \times HOC - f_{NF\_BBOC} \times BBOC - f_{NF\_COC} \times COC - f_{NF\_CCOC}$

360    $\times CCOC) / (SV\text{-}OOC + LV\text{-}OOC)$

361   Here HOC is assumed to originate from gasoline and diesel exhaust and contains

362   exclusively of fossil carbon, i.e., $f_{NF\_HOC} = 0$; BBOC is estimated partly from fossil

363   carbon such as soft coal due to the popular usage in local residents, i.e., $f_{NF\_BBOC} = 1$;

364   COC is assumed to originate from non-fossil carbon such as cooking oil and dressing, i.e.,

365    $f_{NF\_COC} = 1$; CCOC is estimated to originat from coal combustion, i.e., $f_{NF\_CCOC} = 0$.

366

Atmospheric
Chemistry
and Physics
Discussions

3 Results and discussions

367

368   3.1   Overview of field study

369   3.1.1   Meteorological conditions

370   Fig. 1 shows the time series of meteorological parameters and PM_1 components during

371   January 10–February 4, 2014. During the campaign, the measurement site mainly

372   received air masses from northern and northwestern associated with low wind speeds (on

373   average: 0.8 ± 0.4 m s^{-1}). The wind directions were associated with the typical

374   anticyclone mesoscale weather forced by Tibetan Plateau in Lanzhou during winter. The

375   mountains to the north and south of the city significantly reduced the wind speed. Air

376   temperature was typical in winter of Lanzhou ranging from −10 to 14 °C (average = $0.5 \pm$

377   5.0 °C), but was a little warmer after the Chinese New Year (January 31, 2014) (Fig. 1a).

378   No precipitation event occurred during the campaign, and RH was pretty low ranging

379   from 8.8 to 50.7% (avg. = $27.7 \pm 9.1\%$). The visibility ranged from 3.7 to 50 km (avg. =

380   16.0 ± 8.7 km).

381

382   3.1.2   Inter-comparisons

383   The inter-comparisons between AMS *vs*. SMPS and TEOM are shown in Fig. S3.

384   Comparison between the mass concentration of PM_1 and the volume of particle measured

385   by SMPS is tightly correlated ($R^2 = 0.9$) with a slope of 1.48, which represents the

386   average density of bulk particles, assuming that the AMS and the SMPS measure a

387   similar particle population. This value is indeed very close to the estimated PM_1 density

388   (1.46) based on the measured particle composition for this study (using density of 1.2 g

389   m^{-3} for organics, 1.72 g m^{-3} for NH_4NO_3, 1.77 g m^{-3} for $(NH_4)_2SO_4$, 1.52 g m^{-3} for NH_4Cl

390   and 1.8 g m^{-3} for BC) (Zhang et al., 2005; Bond and Bergstrom, 2006). The mass

391   concentration of PM_1 is also closely correlated ($R^2 = 0.71$) with TEOM $PM_{2.5}$

392   concentrations with a slope of 0.73. Similar contribution of PM_1 to $PM_{2.5}$ were also

393   observed in other cities in China during winter (Elser et al., 2016), such as Beijing (0.74

394   during 2011) (Sun et al., 2013b). Note that the actual mass ratio between PM_1 and $PM_{2.5}$

14

395   should be higher than these values since refractory materials such as crustal components

396   were not measured.

397

398   3.1.3 PM_1 composition, variation, and acidity

399   The average mass concentration of PM_1 (NR-PM_1 + BC) was 57.3 µg m^{-3} (ranging from

400   2.1 to 229.7 µg m^{-3} for hourly average) during this study, with 51.2% of organics, 16.5%

401   of nitrate, 12.5% of sulphate, 10.3% of ammonium, 6.4% of BC, and 3.0% of chloride

402   (Fig. 2a). The average mass concentration was more than twice the average value

403   observed during summer 2012 (24.5 µg m^{-3}). All species showed similar day-to-day

404   variation with nitrate being the most significant one (Fig. 1d), suggesting an important

405   local source for nitrate. The mass contributions of PM_1 species from low to high PM_1

406   concentrations showed an increased contribution for organics (49% to 53%) and nitrate

407   (13% to 18%), but a decreased contribution for sulphate (17% to 11%) and BC (7.3% to

408   5.3%) suggesting somewhat different chemical processes/sources for each species during

409   the haze pollution (Fig. 2b). Specifically, the increased organics was mainly due to the

410   contribution of primary OA (POA) based on PMF analysis (more discussion are given in

411   section 3.5). During the late part of Chinese New Year holiday (February 3 to end of the

412   study), PM_1 concentration decreased in association with increased wind speed. NR-PM_1

413   appeared to be neutralized throughout this study, as indicated by an overall stoichiometric

414   charge balance between the anions (i.e., nitrate, sulphate, and chloride) and the cation

415   ammonium (slope = 0.94, Fig. S4). This result indicates that the inorganic particulate

416   species were mainly present in the forms of NH_4NO_3, $(NH_4)_2SO_4$, and NH_4Cl in PM_1.

417

418   3.1.4   Size distribution

419   The average chemically-resolved size distributions of NR-PM_1 species are shown in Fig.

420   3a. While all components peaked between 400–500 nm, organic aerosol presented a

421   wider distribution than the inorganics and extended to ~250 nm, suggesting the influence

422   of fresh organics (primary OA, more discussion are given in section 3.4). These features

423   were similar to those found in most urban sites by the AMS. The similar mode size of

Atmospheric
Chemistry
and Physics
Discussions

424   inorganics and SOA (Fig. 3c) suggested the well external mixed air mass during the

425   sampling period. The mass contributions of chemicals at the major peak (400–500 nm)

426   were organics (~50%), nitrate (~20%), ammonium (~15%), sulphate (~10%), and

427   chloride (~5%); while the contribution of organics increased with the decreasing of size

428   mode (Fig. 3c). Comparing with the results observed during 2012 summer, the size

429   distributions of aerosol particle during winter were narrower, although the mode sizes of

430   major peaks were similar, indicating highly mixed and aged aerosol particles during

431   winter.

432

433   3.2   Diurnal variations of aerosol species

434   All species show significant diurnal variations during the study suggesting the important

435   local and regional sources of aerosol (Fig. 4). The observed diurnal trends of BC

436   presented two dominant peaks with one at late morning (10:00–12:00) and another at

437   early evening (20:00–22:00). The morning peak did not overlap with the rush hours

438   (7:00–9:00), different than that of summer 2012; the BC mass loading started to increase

439   from 6:00 continuously during morning, and reached maximum between 10:00–12:00

440   and then dropped down after the noon time. Another combustion tracer, carbon monoxide

441   (CO), also showed the similar morning peak (Fig. 5). This morning peak was likely

442   resulted from the formation of inversion layer during winter at Lanzhou which promoted

443   accumulation of air pollutants from enhanced human activities in the morning. This

444   inversion layer frequently formed from night time and diffused after the noon time due to

445   the valley terrain. The temperature profile observed at the suburban Lanzhou (Yuzhong,

446   ~30 km from the sampling site) showed a strong inversion in the low boundary layer

447   during the morning time (Fig. S8). The evening peak of BC could result from increased

448   human activities such as traffic, cooking, and heating coupled with low boundary layer

449   after sunset. Organics had two sharp peaks at the noon time (12:00–13:00) and early

450   evening (19:00–20:00) which correspond to lunch time and dinner time, respectively,

451   indicating the importance of cooking-related emissions of OA. PMF analysis show that

Atmospheric
Chemistry
and Physics
Discussions

452   cooking-emitted aerosol could contribute up to 30 – 60% of organics during meal times

453   (section 3.4.3).

454

455   Sulphate presented two peaks with one occurring at the noon time (11:00–14:00) in

456   accordance with the photochemical processes; this peak is narrower than that during

457   summer, likely due to relatively weak photochemical activities. Another minor peak

458   occurred between 20:00–22:00 which was likely due to the lowered boundary layer depth.

459   The significantly higher concentration of sulphate during winter than summer suggests a

460   higher precursor SO_2 emission and stagnant atmospheric conditions in winter. The

461   diurnal pattern of sulphate during winter was similar to that of summer 2012 at Lanzhou

462   and summer 2011 at Beijing, but was different from that of Beijing during winter

463   2011/2012 where aqueous processing was found to could play an important role (Sun et

464   al., 2013b). Chloride had similar diurnal pattern with sulphate, although the evening peak

465   was more obvious. The major source of hydrochloric acid is biomass burning, coal

466   combustion and waste combustion (Ianniello et al., 2011). The significant evening peak

467   could be related with these sources coupled with the shallow boundary layer. The high

468   background concentrations of chloride during day and night suggest a persistent emission

469   of hydrochloric acid which could be from the heating factory and power plants. The

470   diurnal pattern of chloride during winter was different from that during summer 2012

471   which peaked during the night time due to temperature-dependent gas-particle

472   partitioning. Nitrate peaked between 12:00–16:00, right after the peak of sulphate. The

473   formation of nitrate during afternoon suggests that nitrate was dominated by the

474   homogeneous photochemical production. Fig. 5 shows the variations of NO_x and O_3

475   calculated from data downloaded from one station monitored by the Ministry of

476   Environmental Protection of China, ~3 km southwest of sampling site (Fig. S1a); NO had

477   a morning peak (7:00–10:00) and an evening peak (19:00–21:00) corresponding to rush

478   hours; NO_2 increased from 10:00 which formed from NO consumed by OH radical and

479   decreased from 14:00 corresponding to the formation of nitrate and O_3 during afternoon.

480   The diurnal change of NO_x (ΔNO_x) mixing ratio was ~50 ppbv (from 150 to 100 ppbv),

481   while the diurnal change of the sum of ΔO_3 and ΔNO_3^- was ~30 ppbv. Considering the

Atmospheric
Chemistry
and Physics
Discussions

Open Access

482   higher mixing layer height during afternoon, it seems that nitrate was mainly formed

483   from the photochemical processing of NOx. The diurnal pattern of nitrate during winter

484   was vastly different from that during 2012 summer which was mainly controlled by the

485   dynamic of mixing layer and gas-particle partitioning. It seems that atmospheric

486   ammonia was first neutralized by sulphuric acid and hydrochloric acid to form

487   ammonium sulphate and ammonium chloride, and the remaining ammonia may then

488   combine with nitric acid to form ammonium nitrate.

489

490   3.3   Bulk characteristics and elemental ratios of OA

491   Table 1 shows the average elemental mass composition and mass contributions of six ion

492   categories to the total organics. Carbon contributed 66% to the organics following by

493   oxygen (25%), hydrogen (8%), and nitrogen (1%); correspondingly, $C_xH_y^+$ dominated the

494   organics by 59%, following by $C_xH_yO_1^+$ (26%), $C_xH_yO_2^+$ (10%), $H_yO_1^+$ (2%), and

495    $C_xH_yN_p^+$ (2%). Compared with the results of 2012 summer, the organics in winter had

496   higher carbon (66% *vs.* 59%) and $C_xH_y^+$ content (59% *vs.* 56%), and lower oxygen

497   content (25% *vs.* 26%) (Fig. 6c); this suggests that the organics during winter had a

498   higher fraction of primary compounds than those during summer which is likely due to

499   weaker photochemical activities, lower boundary layer height and more emissions from

500   primary sources. The average O/C of organics, an indicator for oxidation state, was 0.28

501   during this study which was somewhat lower than that of summer 2012 (0.33) (Fig. 6a

502   and b). Photochemical processing of organics during winter appeared to be significantly

503   weaker and shorter than those during summer as shown by the diurnal pattern of O/C (Fig.

504   6d). The diurnal profile of H/C was inversely correlated with that of O/C, and the peaking

505   of organic aerosol concentration usually corresponded to the high H/C ratio and low O/C

506   ratio, indicating the dominant role of primary OA.

507

508   3.4   Source apportionment of OA

509   Source apportionment via PMF with ME2 engine on OA mass spectra resolved six

510   components, i.e., HOA, COA, CCOA, BBOA, SV-OOA, and LV-OOA. Each component

Atmospheric
Chemistry
and Physics
Discussions

511 has a unique mass spectral pattern, diurnal pattern, and temporary variation which

512 correlated with corresponding tracers such as inorganic species. Two OOA components

513 can be regarded as surrogates of secondary OA (SOA), with LV-OOA for more aged

514 SOA and SV-OOA for fresher SOA; The HOA, BBOA, COA and CCOA components

515 are regarded as primary OA (POA) based on their low O/C ratios and good correlations

516 with primary aerosol tracers (Fig. 7). Comparison with the source apportionment results

517 of summer 2012, the organic sources and chemical processes during winter 2013/2014

518 were more complex due to the multiple primary sources. Detailed discussion of each

519 factor is given in the following subsections.

520

521 ### 3.4.1 HOA

522 HOA factors had been frequently separated from the OA in urban area due to the

523 emission from traffic and/or other fossil combustion activities (e.g., Sun et al., 2011b; Ge

524 et al., 2012). The diurnal pattern of HOA in winter 2013/2014 of Lanzhou shows two

525 predominant peaks in the morning (10:00–12:00) and evening (20:00–21:00),

526 respectively (Fig. 5). The morning peak started from 6:00 was mainly associated with the

527 morning traffic rush hours, and it maximized at late morning associating with the

528 inversion layer as discussed in Section 3.2. The evening peak was relevant with the

529 evening rush hours and low PBL depth after sunset. The relatively low concentration

530 during afternoon was probably due to the high PBL depth as shown by the mass

531 concentration variations of BC. The correlation between HOA and BC was high ($r = 0.84$,

532 Fig. 7f and Table 2), as a big fraction of BC has been thought to emit from traffic

533 activities and commonly used as a tracer of traffic emission. The minimum of HOA

534 concentration, which typically occurred during afternoon or middle night, was still up to

535 ~2 μg m^{-3} suggesting a high background of HOA which is likely due to the stagnant air

536 condition unfavourable for the diffusion of aerosol. The size distribution of HOA showed

537 a mode size of ~200 nm (Fig. 3b) corresponding to the primary emitted aerosol

538 behaviours and HOA could account for ~25% mass of aerosols between 100-300nm (Fig.

539 3c). The average concentration of HOA during 2013/2014 winter was 2.6 μg m^{-3}

Atmospheric
Chemistry
and Physics
Discussions

540   accounting for 9% of organics (Fig. 8a). This concentration was higher than that of 2012

541   summer in Lanzhou (2.6 *vs*. 1.8 µg m^{-3}) likely due to the lower PBL during winter and

542   stagnant air conditions. The mass contribution from HOA is similar to the result of 2013

543   winter at Beijing (9%) which was also the lowest contributor to the total OA (Sun et al.,

544   2013b; Zhang et al., 2014), probably due to more modern vehicles were used in the past

545   years.

546

547   3.4.2   BBOA

548   BBOA component had been widely observed in USA and European countries during

549   winter due to the traditional wood burning for residential heating (Alfarra et al., 2007).

550   The BBOA component is thought to be less important in China because coal is the major

551   fuel during winter. BBOA could be an important component in China during some

552   special periods. For example, Zhang et al. (2015a) identified a BBOA factor in urban

553   Nanjing, southeast of China, during harvest seasons of summer and autumn because of

554   the burning of straw. The BBOA component has also been identified in some regions in

555   China where the coal resource is scarce. For example, Du et al. (2015) separated a BBOA

556   factor at a rural site of the northern Tibetan Plateau due to the widely usage of cow dung

557   cake for heating in this region. The BBOA component has also been identified during

558   winter in cities in southern China because of rich wood resource in these regions (He et

559   al., 2011; Huang et al., 2011; Huang et al., 2013). To our knowledge, only two recently

560   papers have reported the identification of a BBOA factor during winter using online

561   measurement in an urban area of northern China (Elser et al., 2016). Although the high

562   contribution of non-fossil carbonaceous aerosol was found (Zhang et al., 2015) and the

563   mass spectra of organic in other cities (such as Beijing) during winter have also

564   significant contributions from m/z 60 and 73 (Sun et al., 2013b; Zhang et al., 2014), it is

565   difficult to separate the BBOA using general PMF because of its similar temporal

566   variation with CCOA, such as diurnal pattern (Fig. 4). BBOA contributions presented a

567   clear periodic change (Fig. 1), and on average were high during night time and low

568   during daytime (Fig. 5). This trend is consistent with conventional usage of biomass for

Atmospheric
Chemistry
and Physics
Discussions

Open Access

EGU

569   heating. The time series of BBOA was also closely correlated with BC and chloride

570   (Table 2) due to significant emission of these species from biomass burning. The average

571   mass concentration of BBOA was 3.2 μg m^{-3}, on average contributing 11% of the total

572   OA mass for the entire study (Fig. 8a), but could reach up to 20% during night and down

573   to less than 5% during afternoon (Fig. 8b). This average concentration was close to the

574   results observed at southern Chinese cities such as Jiaxing (~3.9 μg m^{-3}) (Huang et al.,

575   2013), Kaiping (~1.36 μg m^{-3}) (Huang et al., 2011) and Shenzhen (~5.2 μg m^{-3}) (He et

576   al., 2011).

577

578   The size distribution of BBOA peaked at ~400nm which is close to accumulation mode

579   (Fig. 3b). This feature suggests that the BBOA factor observed during this study was

580   likely aged. This behaviour has been observed in some studies and two BBOA factors

581   were identified as a result: one fresh BBOA and one aged BBOA (Zhang et al., 2015a).

582   The relative high O/C and the dominance of an accumulation mode in the size

583   distribution of BBOA were also observed during winter in Fresno, a major city in the

584   Central Valley of California, USA (Ge et al., 2012; Young et al., 2015). These

585   observations are consistent with recent observations that levogolucosan, a major product

586   of biomass burning, can be quickly (within a few hours) oxidized once in the atmosphere

587   (Bougiatioti et al., 2014). Due to the mean RH during the whole study was lower than

588   30%, it seems that biomass emissions were oxidized mostly in the gas phase and the

589   oxidize products subsequently partitioned into the particle phase (Qin and Prather, 2006).

590

591   3.4.3   COA

592   The COA component has been widely identified in urban AMS studies and observational

593   results by other instruments recently, and it is regarded as important source of OA in

594   urban areas (Abdullahi et al., 2013 and references therein). The MS of COA in this study

595   had a major contribution from $C_xH_y^+$ ions (79.7%) with also an important contribution

596   from $C_xH_yO_1^+$ ions (15.5%), similar as those in HOA (80.6% and 13.7%) (Fig. S9). In

597   comparison with the HOA spectrum, COA had a higher m/z 55 to 57 ratio (2.1 vs. 0.7)

Atmospheric
Chemistry
and Physics
Discussions

598   (Fig. 7) which had been postulated as a significant indicator for COA (Sun et al., 2011b;

599   Mohr et al., 2012). In the V-shape plot defined by Mohr et al. (2012), which uses f55 $vs.$

600   f57 after subtracting the contributions from factors of OOA, CCOA, and BBOA (denoted

601   as OOA_CCOA_BOA_sub, i.e. f55$_{OOA_CCOA_BBOA_sub}$ and f57$_{OOA_CCOA_BBOA_sub}$), the data

602   can be clearly represented with ones during morning close to HOA line and ones during

603   meal times close to COA line (Fig. S10). The MS of COA is highly similar to that of

604   summer 2012 observation (R^2 = 0.95, slope = 0.97, Fig. S11) which was found to

605   resemble closely the COA MS from other locations (Xu et al., 2014). In fact, the COA

606   components were found to be associated with heating of cooking oils rather than burning

607   of meat/food itself, and indeed the COA mass spectra from cooking of different dishes

608   were highly similar (He et al., 2010). The O/C and H/C ratios of COA were 0.09 and 1.71,

609   respectively, suggesting its feature as POA. This O/C ratio was slightly lower (0.09 vs.

610   0.11) and the H/C was slightly higher than that of 2012 summer (1.71 vs. 1.69). The size

611   distribution of COA was also peaking between 100–200 nm similar to that of HOA (Fig.

612   3b). The diurnal variation of COA displayed two predominant peaks standing out at lunch

613   time (12:00–13:00) and dinner time (19:00–20:00), respectively (Fig. 5), and a small

614   breakfast peak (~8:00). This pattern was consistent with that of summer 2012 (Fig. 4)

615   which resulted from the consistent routine life during winter and summer. The enhanced

616   COA concentration at dinner time might be mainly due to the low PBL height and the

617   activity of a formal meal with more attendants and longer time than that of lunch. The

618   temporal variation correlated tightly with $C_6H_{10}O^+$ (R^2 = 0.95, Fig. 8d) which has been

619   reported as the high resolution mass spectral markers for ambient COA (Sun et al., 2011b;

620   Ge et al., 2012).

621

622   The average contribution of COA to organics was 20% (~10–50%) (Fig. 8a) with an

623   average mass concentration of 5.86 μg m^{-3} which was much higher than those of HOA

624   and BBOA. This contribution is similar to those in Beijing during winter (average 19% of

625   OA with a range of 16–30%) (Sun et al., 2013b), Fresno (~19% of OA) (Ge et al., 2012),

626   Barcelona (17% of OA) (Mohr et al., 2012), and Paris (11–17%) (Crippa et al., 2013).

627   This high fraction indicates that COA is an important local source of OA in Lanzhou

628   regardless of clear or hazy periods (section 3.5).

629

630   3.4.4   CCOA

631   A CCOA component had been identified in this study with its MS similar to the OA from

632   coal burning in lab study (Dall'Osto et al., 2013). The MS of CCOA had high signals at

633   m/z 41, 43, 44, 55, 57, 69, 91 and 115 (dominated by $C_xH_y^+$ ions) (Fig. 7i) (Elser et al.,

634   2016). $C_xH_y^+$ ions in total account for 75.3% of CCOA MS, following by $C_xH_yO_1^+$

635   (14.7%) and $C_xH_yO_2^+$ (9.4%). The fractions of $C_xH_y^+$ and $C_xH_yO_1^+$ were similar with

636   those in HOA MS (Fig. S9), but the CCOA MS had high signal intensity at m/z 44

637   (mainly CO_2^+) which is different from that of HOA (Fig. 7). This high CO_2^+ fraction was

638   also observed in CCOA MS in Changdao island in China during winter (Hu et al., 2013).

639   Wang et al. (2015) suggested this high CO_2^+ signal is from the oxidative transformation

640   of the pyrolysis products during coal burning. Zhang et al. (2008) reported that 48–68%

641   of particulate organic matter from coal combustion aerosol is found in the form of

642   organic acids. The O/C ratio is thus higher than that of HOA (0.17 *vs*. 0.10) with a lower

643   H/C ratio (1.67 *vs*. 1.73). The CCOA also locates in a relatively high and left position in

644   the triangle plot defined by Ng et al. (2010) (Fig. 13a). These features indicate CCOA is a

645   POA factor but is more oxygenated than HOA. The time-dependent concentrations of

646   CCOA correlated with BC ($r = 0.74$) and chloride ($r = 0.62$) which also correlated well

647   with HOA and BBOA (Table 2). The CCOA mass loading remained high from 20:00 to

648   10:00, slowly decreased to a minimum at 16:00, and then increased from 16:00 to 20:00

649   (Fig. 5). This diurnal pattern was similar to that of BBOA which were all mainly emitted

650   from heating. The slower decreasing rate during morning and increasing rate during late

651   afternoon for CCOA than those of BBOA could related with wide usage of coal, such as

652   cooking and power plants. In our summer 2012 observation, we also observed OA signals

653   from coal combustion which have been persistent emitted during the whole year in

654   Lanzhou. The size distribution of CCOA peaked ~450 nm (Fig. 3b), similar with that of

655   BBOA.

656

657   The average CCOA mass concentration was 5.3 μg m^{-3}, accounting for 18% of total OA

658   mass (Fig. 8a). The mass fraction of CCOA could reach to 25% of OA during night and

659   decreased to 3% during afternoon (Fig. 8b). This indicates that CCOA was an important

660   OA component similar as that in Beijing OA (15–55%) (Zhang et al., 2014; Elser et al.,

661   2016), but its mass fraction of PM$_{2.5}$ (~9%) was at the low end of the values observed at

662   Beijing and Xi'an (9–21%) (Huang et al., 2014).

663

664   3.4.5   SV-OOA and LV-OOA

665   Two or more OOA components are commonly separated by PMF in urban areas which

666   correspond to fresh SOA and aged SOA (Jemenez et al., 2009), and the MS of SOA

667   factors all have predominant contributions at m/z 43 and 44. The MS of fresher SOA such

668   as SV-OOA has higher contribution at m/z 43 (mainly $C_2H_3O^+$, accounting for 73% of

669   m/z 43 in this study), while aged SOA such as LV-OOA has higher signal at m/z 44

670   (mainly CO_2^+, accounting for 98% of m/z 44 in this study). The contribution of $C_xH_yO_1^+$

671   in SV-OOA was 35.6% followed by $C_xH_y^+$ (50.1%), $C_xH_yO_2^+$ (9.4%), $H_yO_1^+$ (1.4%),

672     $C_xH_yN_p^+$ (3.0%), and $C_xH_yO_zN_p^+$ (0.4%) (Fig. S9). The O/C ratio of SV-OOA was 0.31

673   and H/C was 1.47 consistent with fresh SOA. The MS of LV-OOA was comprised of

674   22.1% of $C_xH_yO_2^+$, 35.6% of $C_xH_yO_1^+$, 34.5% of $C_xH_y^+$, 5.5% of $H_xO_1^+$, 2.0% of $C_xH_yN_p^+$,

675   and 0.4% of $C_xH_yO_zN_p^+$ (Fig. S9). The O/C and H/C ratios of LV-OOA were 0.67 and

676   1.29, respectively. Compared with those of summer 2012, both O/C and H/C ratios of

677   SV-OOA during winter 2013/2014 were higher (0.31 vs. 0.28 for O/C, 1.47 vs. 1.34 for

678   H/C), while they were both slightly lower for LV-OOA (0.67 vs. 0.68 for O/C and 1.29 vs.

679   1.34 for H/C). These results indicate that the atmospheric oxidation capacity during

680   winter was still very strong. The positions of SV-OOA and LV-OOA in triangle plot of

681   fCO$_2^+$ vs. fC$_2$H$_3$O$^+$ are situated in the upper left corner (Fig. 13a), respectively, suggesting

682   the oxidation evolution of OOA. The MS of SV-OOA and LV-OOA were similar with

683   those of summer 2012 (R^2 = 0.98 for LV-OOA and R^2 = 0.77 for SV-OOA, Fig. S11).

684   Note that the $C_xH_y^+$ ions in SV-OOA were mainly from by m/z 39, 41, 91 and 115 (Fig.

Atmospheric
Chemistry
and Physics
Discussions

685   7h), which were also found to be enriched in coal combustion organic aerosols. This

686   feature is similar to that of summer 2012, potentially suggesting that part of SV-OOA

687   was from further oxidation of CCOA.

688

689   The temporal variations of SV-OOA and LV-OOA were highly correlated with

690   secondary inorganic species: SV-OOA vs. sulphate ($R^2 = 0.79$) and LV-OOA vs. nitrate

691   ($R^2 = 0.71$) (Fig. 7a and b, Table 2). These patterns are somewhat contradictory to

692   previous AMS findings that SV-OOA typically correlates better with nitrate due to their

693   similar semi-volatile characteristics while LV-OOA tends to correlate better with

694   sulphate as they are both low-volatility species. These correlations were indeed observed

695   during the summer study of 2012 (Xu et al., 2014). The behaviours of the two OOA

696   factors during this study were likely due to the low air temperature and low RH

697   conditions which favoured secondary aerosol formation primarily through gas reactions.

698   Ammonium sulphate was quickly formed in the atmosphere than nitrate, and when SO_2

699   was completely consumed, ammonium nitrate would be formed. The concentration of

700   NO_x was higher than SO_2 (120 vs. 35 ppbv) which the consumption of oxidants by

701   sulphate was relatively less. This phenomenon was also observed in winter time of

702   Beijing which showed strong photochemical formation of nitrate during afternoon (Sun et

703   al., 2013b).

704

705   The diurnal variation profiles of SV-OOA and LV-OOA all showed one bump with the

706   SV-OOA peaking between 11:00–14:00 and LV-OOA peaking between 12:00–18:00,

707   suggesting the importance of photochemical processes for both OOA factors. The size

708   distribution of the OOA (SV-OOA + LV-OOA) had a mode size of ~550 nm (Fig. 3b)

709   reflecting the feature as SOA. This size mode is slightly bigger than those of OOA in

710   other studies such as Fresno (460 nm) and Lanzhou summer 2012 (~450 nm) likely due

711   to the high concentration of gas precursors and longer lifecycle of aerosol during winter.

712

Atmospheric
Chemistry
and Physics
Discussions

Open Access

EGU

713　The mass concentrations of SV-OOA and LV-OOA were 7.0 and 5.6 μg m^{-3} with the

714　mass contributions of 24% and 19% to OA, respectively (Fig. 8a). These contributions

715　were lower than those during summer 2012 in Lanzhou (27% for SV-OOA and 32% for

716　LV-OOA) especially for LV-OOA, likely due to the relative weak solar radiation during

717　winter and more primary sources in winter. The diurnal total contribution of OOA (SV-

718　OOA + LV-OOA) varied between 40%−70% (Fig. 8b), suggesting the importance of

719　SOA in the air pollution throughout the day at Lanzhou.

720

721　3.5　Primary and secondary OA

722　As shown in Fig. 2b, the mass fraction of organics increased with the increase of PM$_1$

723　concentration, so it is important to know the relative contributions of primary and

724　secondary OA components during the pollution periods. Fig. 9a shows the scatter plot of

725　SOA (= SV-OOA + LV-OOA) and POA (= HOA + BBOA + COA + CCOA) during this

726　study. It is clear that POA and OOA show correlation during the periods of POA less

727　than ~15 μg m^{-3} associated with low mass fractions of OA. When POA and OA fraction

728　increased significantly, POA and OOA show almost no correlation, indicating the

729　importance of POA in the severe aerosol pollutions in Lanzhou during winter. This is

730　different than the observation from summer 2012, during which SOA had a stable

731　contribution to PM$_1$ (Fig. 9b), due to more complex POA sources and larger contributions

732　from these sources to PM$_1$ mass loading during winter compared to summer. This is even

733　more evident when comparing each POA factor with OA (Fig. 10). The COA had the

734　biggest contribution to the increased organics can explained 56% of the increase of

735　organics, followed by HOA (28%). The components of CCOA and BBOA also had

736　positive contributions to the increase of PM$_1$ mass. However, both OOA components had

737　negative slopes with organics with SV-OOA being the major one, likely suggesting that

738　the formation of SV-OOA might be limited during heavy haze period in Lanzhou since

739　the reduction of solar radiation may to some extent weaken the photochemical oxidation

740　activities. The phenomenon of POA dominating during haze periods is different from the

741　results in other cities in China (Huang et al., 2014). For example, Elser et al. (2016)

26

Atmospheric
Chemistry
and Physics
Discussions

742   found significant increased contribution from SOA and secondary inorganic aerosol

743   during haze periods in 2013/2014 winter in Xi'an and Beijing. This is likely due to the

744   higher RH values in the eastern China which is more favourable for the aqueous-phase

745   production of SOA. Indeed, Sun et al. (2013a) observed significant increase of secondary

746   inorganic aerosol during high RH periods in Beijing.

747

748   The average contribution of POA to organics decreased from 60.0% to 39.3% during

749   Chinese New Year festival of 2014 (Fig. 1) due to the reduced primary aerosol sources

750   such as HOA (9.8% to 3.3%), COA (21.1% to 11.6%), CCOA (18.2% to 15.4%), and

751   BBOA (10.8% to 9.0%). This is an indication that control of cooking activities and traffic

752   emissions in this residential area may be effective strategies for air quality improvement

753   during winter.

754

755   3.6   Fossil and non-fossil OC

756   OC measured by OC/EC analyser on two filters (OC_{filter}) and corresponding AMS

757   (OC_{AMS}) online measured results are shown in Fig. 11a. The average ratio of

758   OC_{AMS}/OC_{filter} was ~1.5 for these two filters likely due to the analytical uncertainties of

759   different instruments (30% for AMS and 20% for OC_{filter}), which was also observed in

760   other studies (Zotter et al., 2014). The data from the ^{14}C measurement for the filter

761   samples are listed in Table S1. The total average of f_{NF} in these four filters was $55 \pm 3\%$,

762   with 54% and 57% for filters during Jan. 15 and Jan. 23, respectively. Comparison with

763   other studies, the average f_{NF} value in this study was lower than those in Xi'an (63%) and

764   Guangzhou (65%), and higher than those in Beijing (42%), while similar with those in

765   Shanghai (51%) during 2012/2013 winter (Zhang et al., 2015). Combining with the f_{NF}

766   value (the total average of f_{NF} for the total average AMS results) and the contributions of

767   fossil (F) POC (HOC and CCOC) and non-fossil (NF) POC (BBOC and COC), the f_F and

768   f_{NF} for SOC could be obtained (Fig. 11b). The average f_F and f_{NF} for POC and SOC are

769   summarized into Fig. 12. The f_F and f_{NF} for POC during Jan. 15 were 47% and 53%,

770   while for SOC were 44% and 56%. For all AMS data, the f_F and f_{NF} in POC were 47%

771   and 53%, while for SOC were 43% and 57%. The F-POC during Jan. 15 was comprised

772   by 21% HOC and 26% CCOC, and NF-POC by 16% BBOC and 37% COC. For all AMS

773   data, the F-POC was comprised by 16% HOC and 31% CCOC, and NF-POC by 17%

774   BBOC and 36% COC.

775

776   3.7   Evolution of OA and relationship between odd oxygen and SOA

777   The evolution of OA chemical composition upon aging has been an important subject

778   which is used to understand the formation of SOA. The methods to characterize this

779   evolution include the application of several specific diagrams, such as the AMS triangle

780   plot (f44 $vs.$ f43 or fCO$_2^+$ $vs.$ fC$_2$H$_3$O$^+$) (Ng et al., 2010). f44 is a tracer for aged OA

781   (mostly CO$_2^+$), while f43 (mostly C$_2$H$_3$O$^+$, with some contribution from C$_3$H$_7^+$) is mainly

782   associated with freshly formed SOA and POA. POA factors are usually located towards

783   the lower and lower-left corner in triangle plot, and with the aging, move up toward the

784   region of SV-OOA indicating by the increased f43 and f44; and with further aging, OA

785   move toward the region of LV-OOA indicating by the increased f44 and decreased f43. In

786   the plot of f44 $vs.$ f43 of this study (Fig. 13a), the data distributed in a narrow space and

787   move up vertically in the triangle space suggesting significant increasing in f44. The data

788   from the low (night time) to the high (afternoon time) f44 value corresponded to the

789   evolution of the photo radiation intensity suggesting the photochemical processes. The

790   LV-OOA lay at the top of the data consistent with its highly oxidized feature, while

791   BBOA, COA, and HOA all lay at the bottom of triangle space. CCOA is above those of

792   other primary factors consistent with the results of high acid contents in coal burning OA.

793   In the plot of fCO$_2^+$ $vs.$ fC$_2$H$_3$O$^+$ (Fig. 13b), most of data moved out of triangle space

794   because of the high contribution of C$_3$H$_7^+$ at m/z 43, especially for data during night time.

795   fCO$_2^+$ and fC$_2$H$_3$O$^+$ both increased before the noon time, after that fC$_2$H$_3$O$^+$ stopped at

796   ~0.05 and fCO$_2^+$ kept increase likely suggesting the evolution of SV-OOA to LV-OOA.

797   In comparison to the results in summer 2012, the data in winter were more concentrated

798   in the triangle space suggesting air masses with similar source contribution during winter.

799

800   In order to understand the possible sources of oxygenated OA, we also compared the

801   diurnal variations between LV-OOA and O_x (Fig. 13c). Both O_x and OOA are products of

802   photochemical reactions and the comparison between O_x and OOA can offer insight into

803   the evolution of OA due to the dependence of the ratio on the VOC species (Herndon et

804   al., 2008), assuming aqueous processing and night time oxidation for OOA were less

805   important, such as during this study due to the low RH. High SOA *vs*. O_x slopes were

806   observed (larger than 0.12 μg m^{-3} ppb^{-1}) where aromatic VOC dominated the

807   photochemical processing, while a low slopes (~0.03 μg m^{-3} ppb^{-1}) were observed where

808   alkene VOCs dominated the photochemical processing (Wood et al., 2010; Hayes et al.,

809   2013). Fig. 13c shows the scatter plot between O_x and LV-OOA and sized by the mass

810   concentration of BBOA. O_x and LV-OOA showed tight correlation (R^2 = 0.9) with a

811   slope of 0.18 μg m^{-3} ppb^{-1} which suggested the aromatic VOCs may be a large

812   contributor to SOA formation. This result was consistent with the distribution of VOC

813   components in China where aromatic VOC is dominant among VOCs in northern China

814   (Zhang et al., 2015b). Liu et al. (2012) suggested that aromatics emissions in Chinese

815   cities had been underestimated in models by a factor 4-10 which could lead to ~50%

816   increase of SOA production. Apart from the sources of coal combustion, biomass

817   burning, and traffic for aromatic VOC emission (Liu et al., 2008), cooking activities had

818   recently been concerned for accounting for aromatic VOC loading. He et al. (2015)show

819   that Chinese cooking can emit amount of alkanes (41.75%), alkenes (27.23%), and

820   aromatics (28.35%). Combining with ^{14}C results, it suggested that sources that emit

821   modern carbon (e.g., cooking and biomass burning) seem to be higher emission of

822   aromatic VOC than traffic and coal combustion together.

823

824   **4   Conclusions**

825   In order to understand the sources and chemical processes of the air pollution during

826   winter in Lanzhou, a field study was conducted at an urban site of Lanzhou during

827   January 10 – February 4, 2014 using a suit of on-line instruments. The results show that

828   the average mass concentration of PM_1 (NR-PM_1 + BC) was 57.3 μg m^{-3} (ranging from

829   2.1 to 229.7 μg m^{-3} for hourly averages), with 51.2% of organics, 16.5% of nitrate,

830   12.5% of sulphate, 10.3% of ammonium, 6.4% of BC, and 3.0% of chloride. These mass

831   loading levels and chemical compositions were similar to those observed in Beijing

832   during winter. The mass concentration of nitrate and organics increased with the increase

833   of PM$_1$ loading, while sulphate decreased, indicating the importance of OA and nitrate

834   during severe air pollution. The size distributions of all the species displayed a moderate

835   size at 400–500 nm, suggesting that aerosol particles were largely externally mixed

836   during winter. All species presented significant diurnal variations. BC had two peaks at

837   10:00–12:00 and 20:00–22:00, respectively. Further analysis indicated that the first peak

838   was resulted from the inversion layer during morning which accumulated the air

839   pollutants from early morning and until the break-up at around noon time. The evening

840   peak of BC was related to human activities such as traffic and coal combustion coupled

841   with the shallow PBL. OA presented two peaks corresponding to lunch and dinner time

842   suggesting cooking to be an important source. Sulphate peaked during the noon time

843   (11:00–14:00) indicating the importance of photochemical processes. Nitrate presented

844   an afternoon peak (12:00–16:00) which indicate the photochemical processing of NOx.

845   PMF analysis of organic mass spectrum with the ME-2 engine identified six organic

846   aerosol sources: i.e., HOA, BBOA, COA, CCOA, SV-OOA, and LV-OOA. POA, which

847   includes HOA, BBOA, COA, and CCOA, accounted for 57% of OA mass and showed an

848   increased in concentration with the increase of PM$_1$ loading. This is an indication that

849   POA emission was one of the main reasons for the occurrence of heavy air pollution

850   episodes. The temporal profile of LV-OOA tightly correlated with that of nitrate, while

851   those of SV-OOA with sulphate correlated. This observation was different than those

852   observed during other studies and during summer at Lanzhou, indicating the importance

853   of photochemistry for nitrate during winter in Lanzhou due to cold air temperature and

854   low RH conditions. ^{14}C analysis of OOC indicated that 57% of the SOC was formed from

855   non-fossil VOC source including biomass burning and cooking.

856

Atmospheric
Chemistry
and Physics
Discussions

Open Access

EGU

857 **Acknowledgements**

Atmospheric
Chemistry
and Physics

Open Access

EGU

Discussions

864 **References**

865

866 Abdullahi, K. L., Delgado-Saborit, J. M., and Harrison, R. M.: Emissions and indoor
867   concentrations of particulate matter and its specific chemical components from
868   cooking: A   review,   Atmos.   Environ.,   71,   260-294,
869   doi:10.1016/j.atmosenv.2013.01.061,2013.

870 Agrios, K., Salazar, G. A., Zhang, Y. L., Uglietti, C., Battaglia, M., Luginbühl, M.,
871   Ciobanu, V. G., Vonwiller, M., and Szidat, S.: Online coupling of pure O_2
872   thermo-optical methods - ^{14}C AMS for source apportionment of carbonaceous
873   aerosols study, Nucl. Instrum. Meth. Phys. Res. B., 361, 288-293,
874   doi:10.1016/j.nimb.2015.06.008, 2015.

875 Aiken, A. C., DeCarlo, P. F., Kroll, J. H., Worsnop, D. R., Huffman, J. A., Docherty, K.
876   S., Ulbrich, I. M., Mohr, C., Kimmel, J. R., Sueper, D., Sun, Y., Zhang, Q.,
877   Trimborn, A., Northway, M., Ziemann, P. J., Canagaratna, M. R., Onasch, T. B.,
878   Alfarra, M. R., Prevot, A. S. H., Dommen, J., Duplissy, J., Metzger, A.,
879   Baltensperger, U., and Jimenez, J. L.: O/C and OM/OC ratios of primary,
880   secondary, and ambient organic aerosols with high-resolution time-of-flight
881   aerosol mass spectrometry, Environ. Sci. Technol., 42, 4478-4485,
882   doi:10.1021/es703009q, 2008.

883 Alfarra, M. R., Prevot, A. S. H., Szidat, S., Sandradewi, J., Weimer, S., Lanz, V. A.,
884   Schreiber, D., Mohr, M., and Baltensperger, U.: Identification of the Mass
885   Spectral Signature of Organic Aerosols from Wood Burning Emissions, Environ.
886   Sci. Technol., 41, 5770-5777, doi:10.1021/es062289b, 2007.

887 Beekmann, M., Prévôt, A. S. H., Drewnick, F., Sciare, J., Pandis, S. N., Denier van der
888   Gon, H. A. C., Crippa, M., Freutel, F., Poulain, L., Ghersi, V., Rodriguez, E.,
889   Beirle, S., Zotter, P., von der Weiden-Reinmüller, S.-L., Bressi, M., Fountoukis,
890   C., Petetin, H., Szidat, S., Schneider, J., Rosso, A., El Haddad, I., Megaritis, A.,
891   Zhang, Q. J., Michoud, V., Slowik, J. G., Moukhtar, S., Kolmonen, P., Stohl, A.,
892   Eckhardt, S., Borbon, A., Gros, V., Marchand, N., Jaffrezo, J. L.,
893   Schwarzenboeck, A., Colomb, A., Wiedensohler, A., Borrmann, S., Lawrence,
894   M., Baklanov, A., and Baltensperger, U.: In situ, satellite measurement and model
895   evidence on the dominant regional contribution to fine particulate matter levels in
896   the Paris megacity, Atmos. Chem. Phys., 15, 9577-9591, doi:10.5194/acp-15-
897   9577-2015, 2015.

898 Bi, J., Huang, J., Hu, Z., Holben, B. N., and Guo, Z.: Investigating the aerosol optical and
899   radiative characteristics of heavy haze episodes in Beijing during January of 2013,
900   J. Geophys. Res., 119, 9884-9900, doi:10.1002/2014JD021757, 2014.

901 Bond, T., and Bergstrom, R.: Light absorption by carbonaceous particles: An
902   investigative   review,   Aerosol.   Sci.   Tech.,   40,   27–67,
903   doi:10.1080/02786820500421521, 2006.

Atmospheric
Chemistry
and Physics
Discussions

904 Bougiatioti, A., Stavroulas, I., Kostenidou, E., Zarmpas, P., Theodosi, C., Kouvarakis,
905   G., Canonaco, F., Prévôt, A. S. H., Nenes, A., Pandis, S. N., and Mihalopoulos,
906   N.: Processing of biomass-burning aerosol in the eastern Mediterranean during
907   summertime, Atmos. Chem. Phys., 14, 4793-4807, doi:10.5194/acp-14-4793-
908   2014, 2014.

909 Canagaratna, M. R., Jayne, J. T., Jimenez, J. L., Allan, J. D., Alfarra, M. R., Zhang, Q.,
910   Onasch, T. B., Drewnick, F., Coe, H., Middlebrook, A., Delia, A., Williams, L.
911   R., Trimborn, A. M., Northway, M. J., DeCarlo, P. F., Kolb, C. E., Davidovits, P.,
912   and Worsnop, D. R.: Chemical and microphysical characterization of ambient
913   aerosols with the aerodyne aerosol mass spectrometer, Mass Spectrom. Rev., 26,
914   185-222, doi:10.1002/mas.20115, 2007.

915 Canagaratna, M. R., Jimenez, J. L., Kroll, J. H., Chen, Q., Kessler, S. H., Massoli, P.,
916   Hildebrandt Ruiz, L., Fortner, E., Williams, L. R., Wilson, K. R., Surratt, J. D.,
917   Donahue, N. M., Jayne, J. T., and Worsnop, D. R.: Elemental ratio measurements
918   of organic compounds using aerosol mass spectrometry: Characterization,
919   improved calibration, and implications, Atmos. Chem. Phys., 15, 253-272,
920   doi:10.5194/acp-15-253-2015, 2015.

921 Canonaco, F., Crippa, M., Slowik, J. G., Baltensperger, U., and Prévôt, A. S. H.: SoFi, an
922   IGOR-based interface for the efficient use of the generalized multilinear engine
923   (ME-2) for the source apportionment: ME-2 application to aerosol mass
924   spectrometer data, Atmos. Meas. Tech., 6, 3649-3661, doi:10.5194/amt-6-3649-
925   2013, 2013.

926 Cao, C., Jiang, W., Wang, B., Fang, J., Lang, J., Tian, G., Jiang, J., and Zhu, T. F.:
927   Inhalable Microorganisms in Beijing's PM2.5 and PM10 Pollutants during a
928   Severe   Smog   Event,   Environ.   Sci.   Technol.,   48,   1499-1507,
929   doi:10.1021/es4048472, 2014.

930 Chan, C. K., and Yao, X.: Air pollution in mega cities in China, Atmos. Environ., 42, 1-
931   42, doi:10.1016/j.atmosenv.2007.09.003, 2008.

932 Crippa, M., Canonaco, F., Lanz, V. A., Äijälä, M., Allan, J. D., Carbone, S., Capes, G.,
933   Ceburnis, D., Dall'Osto, M., Day, D. A., DeCarlo, P. F., Ehn, M., Eriksson, A.,
934   Freney, E., Hildebrandt Ruiz, L., Hillamo, R., Jimenez, J. L., Junninen, H.,
935   Kiendler-Scharr, A., Kortelainen, A. M., Kulmala, M., Laaksonen, A., Mensah,
936   A. A., Mohr, C., Nemitz, E., O'Dowd, C., Ovadnevaite, J., Pandis, S. N., Petäjä,
937   T., Poulain, L., Saarikoski, S., Sellegri, K., Swietlicki, E., Tiitta, P., Worsnop, D.
938   R., Baltensperger, U., and Prévôt, A. S. H.: Organic aerosol components derived
939   from 25 AMS data sets across Europe using a consistent ME-2 based source
940   apportionment approach, Atmos. Chem. Phys., 14, 6159-6176, doi:10.5194/acp-
941   14-6159-2014, 2014.

942 Crippa, M., DeCarlo, P. F., Slowik, J. G., Mohr, C., Heringa, M. F., Chirico, R., Poulain,
943   L., Freutel, F., Sciare, J., Cozic, J., Di Marco, C. F., Elsasser, M., Nicolas, J. B.,
944   Marchand, N., Abidi, E., Wiedensohler, A., Drewnick, F., Schneider, J.,
945   Borrmann, S., Nemitz, E., Zimmermann, R., Jaffrezo, J. L., Prévôt, A. S. H., and

Atmospheric
Chemistry
and Physics
Discussions

946   Baltensperger, U.: Wintertime aerosol chemical composition and source
947   apportionment of the organic fraction in the metropolitan area of paris, Atmos.
948   Chem. Phys., 13, 961-981, doi:10.5194/acp-13-961-2013, 2013.

949 Dall'Osto, M., Ovadnevaite, J., Ceburnis, D., Martin, D., Healy, R. M., O'Connor, I. P.,
950   Kourtchev, I., Sodeau, J. R., Wenger, J. C., and O'Dowd, C.: Characterization of
951   urban aerosol in Cork city (Ireland) using aerosol mass spectrometry, Atmos.
952   Chem. Phys., 13, 4997-5015, doi:10.5194/acp-13-4997-2013, 2013.

953 DeCarlo, P. F., Kimmel, J. R., Trimborn, A., Northway, M. J., Jayne, J. T., Aiken, A. C.,
954   Gonin, M., Fuhrer, K., Horvath, T., Docherty, K. S., Worsnop, D. R., and
955   Jimenez, J. L.: Field-Deployable, High-Resolution, Time-of-Flight Aerosol Mass
956   Spectrometer, Anal. Chem., 78, 8281-8289, doi:10.1021/ac061249n, 2006.

957 Du, W., Sun, Y. L., Xu, Y. S., Jiang, Q., Wang, Q. Q., Yang, W., Wang, F., Bai, Z. P.,
958   Zhao, X. D., and Yang, Y. C.: Chemical characterization of submicron aerosol
959   and particle growth events at a national background site (3295 m a.s.l.) on the
960   Tibetan Plateau, Atmos. Chem. Phys., 15, 10811-10824, doi:10.5194/acp-15-
961   10811-2015, 2015.

962 Elser, M., Huang, R. J., Wolf, R., Slowik, J. G., Wang, Q., Canonaco, F., Li, G., Bozzetti,
963   C., Daellenbach, K. R., Huang, Y., Zhang, R., Li, Z., Cao, J., Baltensperger, U.,
964   El-Haddad, I., and Prévôt, A. S. H.: New insights into pm2.5 chemical
965   composition and sources in two major cities in china during extreme haze events
966   using aerosol mass spectrometry, Atmos. Chem. Phys., 16, 3207-3225,
967   doi:10.5194/acp-16-3207-2016, 2016.

968 Gao, X., Yang, L., Cheng, S., Gao, R., Zhou, Y., Xue, L., Shou, Y., Wang, J., Wang, X.,
969   Nie, W., Xu, P., and Wang, W.: Semi-continuous measurement of water-soluble
970   ions in PM2.5 in Jinan, China: Temporal variations and source apportionments,
971   Atmos. Environ., 45, 6048-6056, doi:10.1016/j.atmosenv.2011.07.041, 2011.

972 Ge, X., Setyan, A., Sun, Y., and Zhang, Q.: Primary and secondary organic aerosols in
973   Fresno, California during wintertime: Results from high resolution aerosol mass
974   spectrometry, J. Geophys. Res., 117, D19301, doi:10.1029/2012jd018026, 2012.

975 Hayes, P. L., Ortega, A. M., Cubison, M. J., Froyd, K. D., Zhao, Y., Cliff, S. S., Hu, W.
976   W., Toohey, D. W., Flynn, J. H., Lefer, B. L., Grossberg, N., Alvarez, S.,
977   Rappenglück, B., Taylor, J. W., Allan, J. D., Holloway, J. S., Gilman, J. B.,
978   Kuster, W. C., de Gouw, J. A., Massoli, P., Zhang, X., Liu, J., Weber, R. J.,
979   Corrigan, A. L., Russell, L. M., Isaacman, G., Worton, D. R., Kreisberg, N. M.,
980   Goldstein, A. H., Thalman, R., Waxman, E. M., Volkamer, R., Lin, Y. H., Surratt,
981   J. D., Kleindienst, T. E., Offenberg, J. H., Dusanter, S., Griffith, S., Stevens, P. S.,
982   Brioude, J., Angevine, W. M., and Jimenez, J. L.: Organic aerosol composition
983   and sources in Pasadena, California during the 2010 CalNex campaign, J.
984   Geophys. Res., 118, 9233-9257, doi:10.1002/jgrd.50530, 2013.

985 He, K., Yang, F., Ma, Y., Zhang, Q., Yao, X., Chan, C. K., Cadle, S., Chan, T., and
986   Mulawa, P.: The characteristics of PM2.5 in Beijing, China, Atmos. Environ., 35,
987   4959-4970, doi:10.1016/s1352-2310(01)00301-6, 2001.

Atmospheric
Chemistry
and Physics
Discussions

988   He, L.-Y., Huang, X.-F., Xue, L., Hu, M., Lin, Y., Zheng, J., Zhang, R., and Zhang, Y.-
989   H.: Submicron aerosol analysis and organic source apportionment in an urban
990   atmosphere in Pearl River Delta of China using high-resolution aerosol mass
991   spectrometry, J. Geophys. Res., 116, D12304, doi:10.1029/2010jd014566, 2011.

992   He, L. Y., Lin, Y., Huang, X. F., Guo, S., Xue, L., Su, Q., Hu, M., Luan, S. J., and Zhang,
993   Y. H.: Characterization of high-resolution aerosol mass spectra of primary organic
994   aerosol emissions from Chinese cooking and biomass burning, Atmos. Chem.
995   Phys., 10, 11535-11543, doi:10.5194/acp-10-11535-2010, 2010.

996   He, Q., Yan, Y., Li, H., Zhang, Y., Chen, L., and Wang, Y.: Characteristics and reactivity
997   of volatile organic compounds from non-coal emission sources in China, Atmos.
998   Environ., 115, 153-162, doi:10.1016/j.atmosenv.2015.05.066, 2015.

999   Herndon, S. C., Onasch, T. B., Wood, E. C., Kroll, J. H., Canagaratna, M. R., Jayne, J.
1000   T., Zavala, M. A., Knighton, W. B., Mazzoleni, C., Dubey, M. K., Ulbrich, I. M.,
1001   Jimenez, J. L., Seila, R., de Gouw, J. A., de Foy, B., Fast, J., Molina, L. T., Kolb,
1002   C. E., and Worsnop, D. R.: Correlation of secondary organic aerosol with odd
1003   oxygen   in   Mexico   City,   Geophys.   Res.   Lett.,   35,   L15804,
1004   doi:10.1029/2008GL034058, 2008.

1005 Hu, W. W., Hu, M., Yuan, B., Jimenez, J. L., Tang, Q., Peng, J. F., Hu, W., Shao, M.,
1006   Wang, M., Zeng, L. M., Wu, Y. S., Gong, Z. H., Huang, X. F., and He, L. Y.:
1007   Insights on organic aerosol aging and the influence of coal combustion at a
1008   regional receptor site of central eastern China, Atmos. Chem. Phys., 13, 10095-
1009   10112, doi:10.5194/acp-13-10095-2013, 2013.

1010 Huang, R.-J., Zhang, Y., Bozzetti, C., Ho, K.-F., Cao, J.-J., Han, Y., Daellenbach, K. R.,
1011   Slowik, J. G., Platt, S. M., Canonaco, F., Zotter, P., Wolf, R., Pieber, S. M.,
1012   Bruns, E. A., Crippa, M., Ciarelli, G., Piazzalunga, A., Schwikowski, M.,
1013   Abbaszade, G., Schnelle-Kreis, J., Zimmermann, R., An, Z., Szidat, S.,
1014   Baltensperger, U., Haddad, I. E., and Prevot, A. S. H.: High secondary aerosol
1015   contribution to particulate pollution during haze events in China, Nature, 514,
1016   218-222, doi:10.1038/nature13774, 2014

1017 Huang, X.-F., Xue, L., Tian, X.-D., Shao, W.-W., Sun, T.-L., Gong, Z.-H., Ju, W.-W.,
1018   Jiang, B., Hu, M., and He, L.-Y.: Highly time-resolved carbonaceous aerosol
1019   characterization in Yangtze River Delta of China: Composition, mixing state and
1020   secondary   formation,   Atmos.   Environ.,   64,   200-207,
1021   doi:10.1016/j.atmosenv.2012.09.059, 2013.

1022 Huang, X. F., He, L. Y., Hu, M., Canagaratna, M. R., Kroll, J. H., Ng, N. L., Zhang, Y.
1023   H., Lin, Y., Xue, L., Sun, T. L., Liu, X. G., Shao, M., Jayne, J. T., and Worsnop,
1024   D. R.: Characterization of submicron aerosols at a rural site in Pearl River Delta
1025   of China using an Aerodyne High-Resolution Aerosol Mass Spectrometer, Atmos.
1026   Chem. Phys., 11, 1865-1877, doi:10.5194/acp-11-1865-2011, 2011.

1027 Ianniello, A., Spataro, F., Esposito, G., Allegrini, I., Hu, M., and Zhu, T.: Chemical
1028   characteristics of inorganic ammonium salts in PM2.5 in the atmosphere of

Atmospheric
Chemistry
and Physics
Discussions

1029   Beijing (China), Atmos. Chem. Phys., 11, 10803-10822, doi:10.5194/acp-11-
1030   10803-2011, 2011.

1031   Jayne, J. T., Leard, D. C., Zhang, X., Davidovits, P., Smith, K. A., Kolb, C. E., and
1032   Worsnop, D. R.: Development of an Aerosol Mass Spectrometer for Size and
1033   Composition Analysis of Submicron Particles, Aerosol. Sci. Tech., 33, 49 - 70,
1034   doi:10.1080/027868200410840, 2000.

1035   Jimenez, J. L., Canagaratna, M. R., Donahue, N. M., Prevot, A. S. H., Zhang, Q., Kroll, J.
1036   H., DeCarlo, P. F., Allan, J. D., Coe, H., Ng, N. L., Aiken, A. C., Docherty, K. S.,
1037   Ulbrich, I. M., Grieshop, A. P., Robinson, A. L., Duplissy, J., Smith, J. D.,
1038   Wilson, K. R., Lanz, V. A., Hueglin, C., Sun, Y. L., Tian, J., Laaksonen, A.,
1039   Raatikainen, T., Rautiainen, J., Vaattovaara, P., Ehn, M., Kulmala, M.,
1040   Tomlinson, J. M., Collins, D. R., Cubison, M. J., E., Dunlea, J., Huffman, J. A.,
1041   Onasch, T. B., Alfarra, M. R., Williams, P. I., Bower, K., Kondo, Y., Schneider,
1042   J., Drewnick, F., Borrmann, S., Weimer, S., Demerjian, K., Salcedo, D., Cottrell,
1043   L., Griffin, R., Takami, A., Miyoshi, T., Hatakeyama, S., Shimono, A., Sun, J. Y.,
1044   Zhang, Y. M., Dzepina, K., Kimmel, J. R., Sueper, D., Jayne, J. T., Herndon, S.
1045   C., Trimborn, A. M., Williams, L. R., Wood, E. C., Middlebrook, A. M., Kolb, C.
1046   E., Baltensperger, U., and Worsnop, D. R.: Evolution of organic aerosols in the
1047   atmosphere, Science, 326, 1525-1529, doi:10.1126/science.1180353, 2009.

1048   Liu, Y., Shao, M., Fu, L., Lu, S., Zeng, L., and Tang, D.: Source profiles of volatile
1049   organic compounds (VOCs) measured in China: Part I, Atmos. Environ., 42,
1050   6247-6260, doi:10.1016/j.atmosenv.2008.01.070, 2008.

1051   Liu, Z., Wang, Y., Vrekoussis, M., Richter, A., Wittrock, F., Burrows, J. P., Shao, M.,
1052   Chang, C.-C., Liu, S.-C., Wang, H., and Chen, C.: Exploring the missing source
1053   of glyoxal (CHOCHO) over China, Geophys. Res. Lett., 39, L10812,
1054   doi:10.1029/2012GL051645, 2012.

1055   Minguillón, M. C., Perron, N., Querol, X., Szidat, S., Fahrni, S. M., Alastuey, A.,
1056   Jimenez, J. L., Mohr, C., Ortega, A. M., Day, D. A., Lanz, V. A., Wacker, L.,
1057   Reche, C., Cusack, M., Amato, F., Kiss, G., Hoffer, A., Decesari, S., Moretti, F.,
1058   Hillamo, R., Teinilä, K., Seco, R., Peñuelas, J., Metzger, A., Schallhart, S.,
1059   Müller, M., Hansel, A., Burkhart, J. F., Baltensperger, U., and Prévôt, A. S. H.:
1060   Fossil versus contemporary sources of fine elemental and organic carbonaceous
1061   particulate matter during the DAURE campaign in Northeast Spain, Atmos.
1062   Chem. Phys., 11, 12067-12084, doi:10.5194/acp-11-12067-2011, 2011.

1063   Mohr, C., DeCarlo, P. F., Heringa, M. F., Chirico, R., Slowik, J. G., Richter, R., Reche,
1064   C., Alastuey, A., Querol, X., Seco, R., Penuelas, J., Jimenez, J. L., Crippa, M.,
1065   Zimmermann, R., Baltensperger, U., and Prevot, A. S. H.: Identification and
1066   quantification of organic aerosol from cooking and other sources in Barcelona
1067   using aerosol mass spectrometer data, Atmos. Chem. Phys., 12, 1649-1665,
1068   doi:10.5194/acp-12-1649-2012, 2012.

1069   Ng, N. L., Canagaratna, M. R., Zhang, Q., Jimenez, J. L., Tian, J., Ulbrich, I. M., Kroll, J.
1070   H., Docherty, K. S., Chhabra, P. S., Bahreini, R., Murphy, S. M., Seinfeld, J. H.,

1071   Hildebrandt, L., Donahue, N. M., DeCarlo, P. F., Lanz, V. A., Prévôt, A. S. H.,
1072   Dinar, E., Rudich, Y., and Worsnop, D. R.: Organic aerosol components observed
1073   in Northern Hemispheric datasets from Aerosol Mass Spectrometry, Atmos.
1074   Chem. Phys., 10, 4625-4641, doi:10.5194/acp-10-4625-2010, 2010.

1075   Paatero, P., and Tapper, U.: Positive matrix factorization: A non-negative factor model
1076   with optimal utilization of error estimates of data values, Environmetrics, 5,
1077   doi:111-126, 10.1002/env.3170050203, 1994.

1078   Qin, X., and Prather, K. A.: Impact of biomass emissions on particle chemistry during the
1079   California Regional Particulate Air Quality Study, Int. J. Mass. Spectrom., 258,
1080   142-150, doi:10.1016/j.ijms.2006.09.004, 2006.

1081   Song, Y., Xie, S., Zhang, Y., Zeng, L., Salmon, L. G., and Zheng, M.: Source
1082   apportionment of PM2.5 in Beijing using principal component analysis/absolute
1083   principal component scores and UNMIX, Sci. Total. Environ., 372, 278-286,
1084   doi:10.1016/j.scitotenv.2006.08.041, 2006.

1085   Sun, Y., Du, W., Fu, P., Wang, Q., Li, J., Ge, X., Zhang, Q., Zhu, C., Ren, L., Xu, W.,
1086   Zhao, J., Han, T., Worsnop, D. R., and Wang, Z.: Primary and secondary aerosols
1087   in Beijing in winter: sources, variations and processes, Atmos. Chem. Phys.
1088   Discuss., 1-41, 10.5194/acp-2016-255, 2016.

1089   Sun, Y., Jiang, Q., Wang, Z., Fu, P., Li, J., Yang, T., and Yin, Y.: Investigation of the
1090   sources and evolution processes of severe haze pollution in Beijing in January
1091   2013, J. Geophys. Res., 119, 2014JD021641, doi:10.1002/2014JD021641, 2014.

1092   Sun, Y., Zhuang, G., Tang, A., Wang, Y., and An, Z.: Chemical Characteristics of PM2.5
1093   and PM10 in Haze−Fog Episodes in Beijing, Environ. Sci. Technol., 40, 3148-
1094   3155, doi:10.1021/es051533g, 2006.

1095   Sun, Y., Zhang, Q., Zheng, M., Ding, X., Edgerton, E. S., and Wang, X.: Characterization
1096   and source apportionment of water-soluble organic matter in atmospheric fine
1097   particles (pm$_{2.5}$) with high-resolution aerosol mass spectrometry and gc-ms,
1098   Environ. Sci. and Technol., 45, 4854 - 4861, doi:10.1021/es200162h, 2011a.

1099   Sun, Y., Zhang, Q., Schwab, J. J., Demerjian, K. L., Chen, W. N., Bae, M. S., Hung, H.
1100   M., Hogrefe, O., Frank, B., Rattigan, O. V., and Lin, Y. C.: Characterization of
1101   the sources and processes of organic and inorganic aerosols in New York city
1102   with a high-resolution time-of-flight aerosol mass apectrometer, Atmos. Chem.
1103   Phys., 11, 1581-1602, doi:10.5194/acp-11-1581-2011, 2011b.

1104   Sun, Y. L., Wang, Z., Fu, P., Jiang, Q., Yang, T., Li, J., and Ge, X.: The impact of
1105   relative humidity on aerosol composition and evolution processes during
1106   wintertime in Beijing, China, Atmos. Environ., 77, 927-934,
1107   doi:10.1016/j.atmosenv.2013.06.019, 2013a.

1108   Sun, Y. L., Wang, Z. F., Fu, P. Q., Yang, T., Jiang, Q., Dong, H. B., Li, J., and Jia, J. J.:
1109   Aerosol composition, sources and processes during wintertime in Beijing, China,
1110   Atmos. Chem. Phys., 13, 4577-4592, doi:10.5194/acp-13-4577-2013, 2013b.

Atmospheric
Chemistry
and Physics
Discussions

1111 Szidat, S.; Salazar, G. A.; Vogel, E.; Battaglia, M.; Wacker, L.; Synal, H. A.; Türler, A.:
1112 ^{14}C analysis and sample preparation at the new Bern Laboratory for the Analysis
1113   of Radiocarbon with AMS (LARA). Radiocarbon, 56, 561-566,
1114   doi:10.2458/56.17457, 2014.

1115 Ulbrich, I. M., Canagaratna, M. R., Zhang, Q., Worsnop, D. R., and Jimenez, J. L.:
1116   Interpretation of organic components from Positive Matrix Factorization of
1117   aerosol mass spectrometric data, Atmos. Chem. Phys., 9, 2891-2918,
1118   doi:10.5194/acp-9-2891-2009, 2009.

1119 Wang, X., Cotter, E., Iyer, K. N., Fang, J., Williams, B. J., and Biswas, P.: Relationship
1120   between pyrolysis products and organic aerosols formed during coal combustion,
1121   P. Combust. Inst., 35, 2347-2354, doi:10.1016/j.proci.2014.07.073, 2015.

1122 Wang, Y., Ying, Q., Hu, J., and Zhang, H.: Spatial and temporal variations of six criteria
1123   air pollutants in 31 provincial capital cities in China during 2013–2014, Environ.
1124   Int., 73, 413-422, doi:10.1016/j.envint.2014.08.016, 2014.

1125 Wiedensohler, A., Birmili, W., Nowak, A., Sonntag, A., Weinhold, K., Merkel, M.,
1126   Wehner, B., Tuch, T., Pfeifer, S., Fiebig, M., Fjäraa, A. M., Asmi, E., Sellegri, K.,
1127   Depuy, R., Venzac, H., Villani, P., Laj, P., Aalto, P., Ogren, J. A., Swietlicki, E.,
1128   Williams, P., Roldin, P., Quincey, P., Hüglin, C., Fierz-Schmidhauser, R., Gysel,
1129   M., Weingartner, E., Riccobono, F., Santos, S., Grüning, C., Faloon, K.,
1130   Beddows, D., Harrison, R., Monahan, C., Jennings, S. G., O'Dowd, C. D.,
1131   Marinoni, A., Horn, H. G., Keck, L., Jiang, J., Scheckman, J., McMurry, P. H.,
1132   Deng, Z., Zhao, C. S., Moerman, M., Henzing, B., de Leeuw, G., Löschau, G.,
1133   and Bastian, S.: Mobility particle size spectrometers: harmonization of technical
1134   standards and data structure to facilitate high quality long-term observations of
1135   atmospheric particle number size distributions, Atmos. Meas. Tech., 5, 657-685,
1136   doi:10.5194/amt-5-657-2012, 2012.

1137 Wood, E. C., Canagaratna, M. R., Herndon, S. C., Onasch, T. B., Kolb, C. E., Worsnop,
1138   D. R., Kroll, J. H., Knighton, W. B., Seila, R., Zavala, M., Molina, L. T.,
1139   DeCarlo, P. F., Jimenez, J. L., Weinheimer, A. J., Knapp, D. J., Jobson, B. T.,
1140   Stutz, J., Kuster, W. C., and Williams, E. J.: Investigation of the correlation
1141   between odd oxygen and secondary organic aerosol in Mexico City and Houston,
1142   Atmos. Chem. Phys., 10, 8947-8968, doi:10.5194/acp-10-8947-2010, 2010.

1143 Xu, J., Zhang, Q., Chen, M., Ge, X., Ren, J., and Qin, D.: Chemical composition, sources,
1144   and processes of urban aerosols during summertime in northwest China: insights
1145   from high-resolution aerosol mass spectrometry, Atmos. Chem. Phys., 14, 12593-
1146   12611, doi:10.5194/acp-14-12593-2014, 2014.

1147 Xue, J., Griffith, S. M., Yu, X., Lau, A. K. H., and Yu, J. Z.: Effect of nitrate and sulfate
1148   relative abundance in PM2.5 on liquid water content explored through half-hourly
1149   observations of inorganic soluble aerosols at a polluted receptor site, Atmos.
1150   Environ., 99, 24-31, doi:10.1016/j.atmosenv.2014.09.049, 2014.

1151 Young, D., Kim, H. J., Parworth, C., Zhou, S., Zhang, X. L., Cappa, C., Seco, R., Kim,
1152   S., and Zhang, Q.: Influences of emission sources and meteorology on aerosol

Atmospheric
Chemistry
and Physics
Discussions

Open Access

EGU

1153 chemistry in a polluted urban environment: Results from discover-aq california,
1154 Atmospheric   Chemistry   &   Physics   Discussions,   15,   35057-35115,
1155 doi:10.5194/acpd-15-35057-2015, 2015.

1156 Yu, L., Wang, G., Zhang, R., Zhang, L., Song, Y., Wu, B., Li, X., An, K., and Chu, J.:
1157 Characterization and Source Apportionment of PM2.5 in an Urban Environment
1158 in Beijing, Aerosol Air Qual. Res., 13, 574-583, doi:10.4209/aaqr.2012.07.0192,
1159 2013.

1160 Zhang, J. K., Sun, Y., Liu, Z. R., Ji, D. S., Hu, B., Liu, Q., and Wang, Y. S.:
1161 Characterization of submicron aerosols during a month of serious pollution in
1162 Beijing, 2013, Atmos. Chem. Phys., 14, 2887-2903, doi:10.5194/acp-14-2887-
1163 2014, 2014.

1164 Zhang, Q., Canagaratna, M. R., Jayne, J. T., Worsnop, D. R., and Jimenez, J. L.: Time-
1165 and size-resolved chemical composition of submicron particles in Pittsburgh:
1166 Implications for aerosol sources and processes, J. Geophys. Res., 110, D07s09,
1167 doi:10.1029/2004jd004649, 2005.

1168 Zhang, Q., Jimenez, J. L., Canagaratna, M. R., Ulbrich, I. M., Ng, N. L., Worsnop, D. R.,
1169 and Sun, Y.: Understanding atmospheric organic aerosols via factor analysis of
1170 aerosol mass spectrometry: a review, Anal. Bioanal. Chem., 401, 3045-3067,
1171 doi:10.1007/s00216-011-5355-y, 2011a.

1172 Zhang, R., Jing, J., Tao, J., Hsu, S. C., Wang, G., Cao, J., Lee, C. S. L., Zhu, L., Chen, Z.,
1173 Zhao, Y., and Shen, Z.: Chemical characterization and source apportionment of
1174 PM2.5 in Beijing: seasonal perspective, Atmos. Chem. Phys., 13, 7053-7074,
1175 doi:10.5194/acp-13-7053-2013, 2013.

1176 Zhang, Y., Schauer, J. J., Zhang, Y., Zeng, L., Wei, Y., Liu, Y., and Shao, M.:
1177 Characteristics of Particulate Carbon Emissions from Real-World Chinese Coal
1178 Combustion, Environ. Sci. Technol., 42, 5068-5073, doi:10.1021/es7022576,
1179 2008.

1180 Zhang, Y. J., Tang, L. L., Wang, Z., Yu, H. X., Sun, Y. L., Liu, D., Qin, W., Canonaco,
1181 F., Prévôt, A. S. H., Zhang, H. L., and Zhou, H. C.: Insights into characteristics,
1182 sources, and evolution of submicron aerosols during harvest seasons in the
1183 Yangtze River delta region, China, Atmos. Chem. Phys., 15, 1331-1349,
1184 doi:10.5194/acp-15-1331-2015, 2015a.

1185 Zhang, Y. L., Huang, R. J., El Haddad, I., Ho, K. F., Cao, J. J., Han, Y., Zotter, P.,
1186 Bozzetti, C., Daellenbach, K. R., Canonaco, F., Slowik, J. G., Salazar, G.,
1187 Schwikowski, M., Schnelle-Kreis, J., Abbaszade, G., Zimmermann, R.,
1188 Baltensperger, U., Prévôt, A. S. H., and Szidat, S.: Fossil vs. Non-fossil sources of
1189 fine carbonaceous aerosols in four chinese cities during the extreme winter haze
1190 episode of 2013, Atmos. Chem. Phys., 15, 1299-1312, 10.5194/acp-15-1299-
1191 2015, 2015.

1192 Zhang, Y. L.; Perron, N.; Ciobanu, V. G.; Zotter, P.; Minguillón, M. C.; Wacker, L.;
1193 Prévôt, A. S. H.; Baltensperger, U.; Szidat, S.: On the isolation of OC and EC and

Atmospheric
Chemistry
and Physics
Discussions

1194   the optimal strategy of radiocarbon-based source apportionment of carbonaceous
1195   aerosols. Atmos. Chem. Phys., 12, 10841-10856, doi:10.5194/acp-12-10841-
1196   2012, 2012.

1197   Zhang, Y. M., Zhang, X. Y., Sun, J. Y., Lin, W. L., Gong, S. L., Shen, X. J., and Yang,
1198   S.: Characterization of new particle and secondary aerosol formation during
1199   summertime in Beijing, China, Tellus. B, 63, 382-394, doi:10.1111/j.1600-
1200   0889.2011.00533.x, 2011b.

1201   Zhang, Z., Wang, X., Zhang, Y., Lü, S., Huang, Z., Huang, X., and Wang, Y.: Ambient
1202   air benzene at background sites in China's most developed coastal regions:
1203   Exposure levels, source implications and health risks, Sci. Total. Environ., 511,
1204   792-800, doi:10.1016/j.scitotenv.2015.01.003, 2015b.

1205   Zhao, X. J., Zhao, P. S., Xu, J., Meng, W., Pu, W. W., Dong, F., He, D., and Shi, Q. F.:
1206   Analysis of a winter regional haze event and its formation mechanism in the
1207   North China Plain, Atmos. Chem. Phys., 13, 5685-5696, doi:10.5194/acp-13-
1208   5685-2013, 2013.

1209   Zheng, G. J., Duan, F. K., Su, H., Ma, Y. L., Cheng, Y., Zheng, B., Zhang, Q., Huang, T.,
1210   Kimoto, T., Chang, D., Su, H., Pöschl, U., Cheng, Y. F., and He, K. B.: Exploring
1211   the severe winter haze in Beijing: the impact of synoptic weather, regional
1212   transport and heterogeneous reactions. Atmos. Chem. Phys., 15, 2969-2983,
1213   doi:10.5194/acp-15-2969-2015, 2015.

1214   Zheng, M., Salmon, L. G., Schauer, J. J., Zeng, L., Kiang, C. S., Zhang, Y., and Cass, G.
1215   R.: Seasonal trends in PM2.5 source contributions in Beijing, China, Atmos.
1216   Environ., 39, 3967-3976, doi:10.1016/j.atmosenv.2005.03.036, 2005.

1217   Zotter, P., El-Haddad, I., Zhang, Y., Hayes, P. L., Zhang, X., Lin, Y.-H., Wacker, L.,
1218   Schnelle-Kreis, J., Abbaszade, G., Zimmermann, R., Surratt, J. D., Weber, R.,
1219   Jimenez, J. L., Szidat, S., Baltensperger, U., and Prévôt, A. S. H.: Diurnal cycle of
1220   fossil and nonfossil carbon using radiocarbon analyses during CalNex, Journal of
1221   Geophysical   Research: Atmospheres,   119,   6818-6835,
1222   doi:10.1002/2013JD021114, 2014.

Atmospheric
Chemistry
and Physics
Discussions

Open Access

1223

1224   Table 1 Comparison of the composition of category ions and elemental composition of

1225   OA between winter 2013/2014 and summer 2012.

1226

Category Ions	Winter 2014	Summer 2012
$C_xH_y^+$	61%	56%
$C_xH_yO_1^+$	25%	27%
$C_xH_yO_2^+$	9%	11%
$C_xH_yN_p^+$	3%	3%
$C_xH_yN_pO_z^+$	0	1%
$H_yO_1^+$	2%	2%
Elemental composition		
C	66%	59%
H	8%	7%
O	25%	26%
N	1%	1%

1227

1228   Table 2 Correlation coefficient (*r*) between time series of OA factors and other aerosol

1229   species.

r	HOA	BBOA	COA	CCOA	SV-OOA	LV-OOA	POA*	SOA*
BC	**0.84**	0.75	0.43	**0.74**	0.59	0.14	**0.75**	0.44
PAH	0.69	0.75	0.46	0.73	0.27	-0.07	**0.75**	0.13
Sulphate	0.69	0.35	0.32	0.32	**0.89**	0.56	0.49	**0.84**
Nitrate	0.35	0.06	0.31	0.06	**0.77**	**0.84**	0.31	**0.90**
Chloride	0.75	0.62	0.33	0.62	**0.79**	0.30	0.61	0.64
Sulphate + Nitrate	0.50	0.17	0.34	0.16	**0.86**	**0.79**	0.40	**0.93**
Sulphate + Nitrate + Chloride	0.59	0.29	0.35	0.29	**0.89**	**0.70**	0.47	**0.91**

1230   * POA = HOA + BBOA + COA + CCOA, SOA = SV-OOA + LV-OOA

1231

Atmospheric
Chemistry
and Physics
Discussions
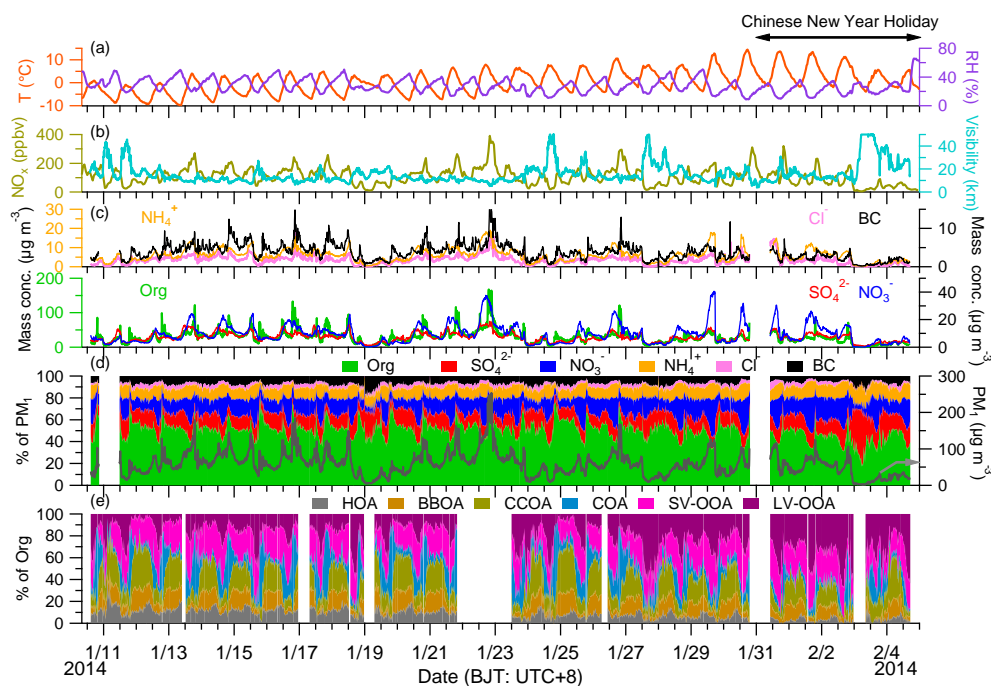
1232
1233
Fig. 1 Summary of meteorological and aerosol species data. (a) air temperature (T) and relative humidity (RH), (b) NOx and visibility, (c) mass concentration of PM$_1$ species, (d) the mass contribution of PM1 species, and (e) the mass contribution of organic components to organic aerosol.

1238

Atmospheric
Chemistry
and Physics
Discussions

1239
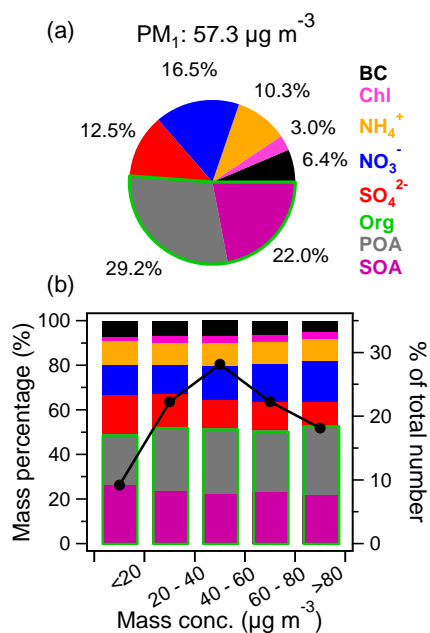
1240
1241
1242   Fig. 2 The average mass contribution of PM_1 (= NR-PM_1 + BC) species (a) during the

1243   whole sampling period and (b) as a function of the PM_1 mass concentration ($\mu g\ m^{-3}$) bins

1244   (left). The right axis in (b) shows the accumulated data number in each bin. The organics

1245   were decomposed into primary oganic aerosol (POA) and secondary organic aerosol

1246   (SOA) using PMF (section 3.4).

1247

Atmospheric
Chemistry
and Physics
Discussions
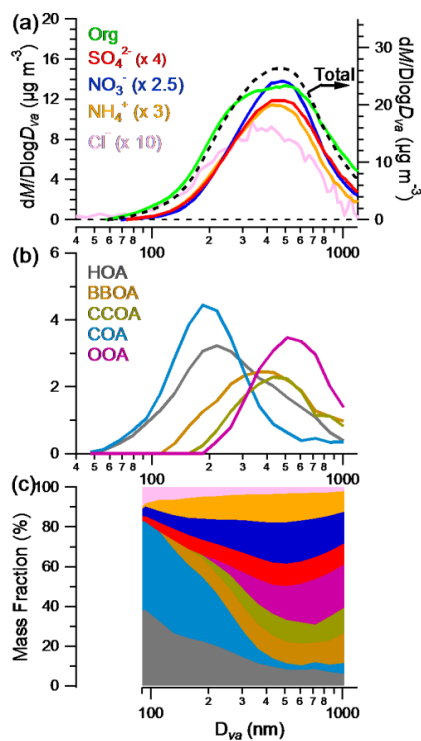
1248

1249   Fig. 3 The size distributions of (a) NR-PM$_1$ species, (b) organic components, and mass

1250   contribution of all species to NR-PM$_1$.

1251

Atmospheric
Chemistry
and Physics
Discussions
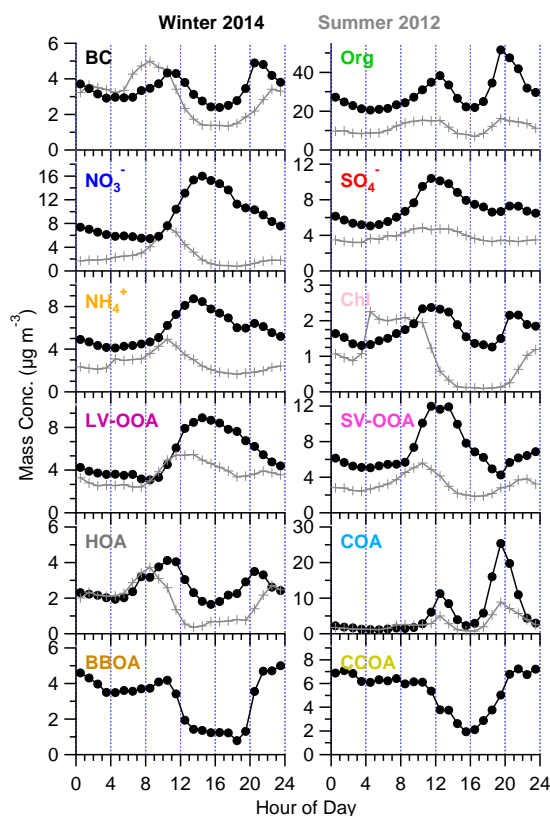
1252

Fig. 4 The diurnal variation of PM_1 species during winter 2013/2014 and summer 2012.

1253

1254
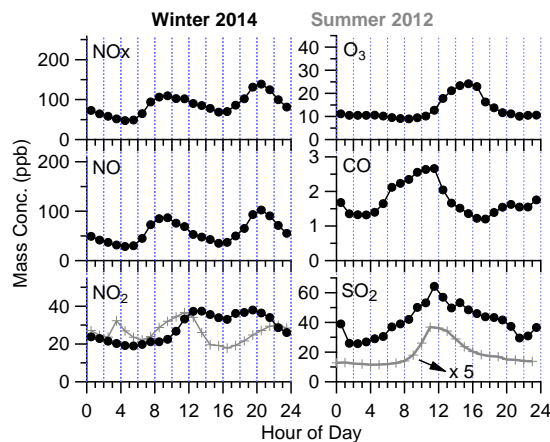
1255

1256   Fig. 5 The diurnal variations of gas species downloaded from MAP-China station during

1257   winter 2013/2014 and summer 2012.

1258
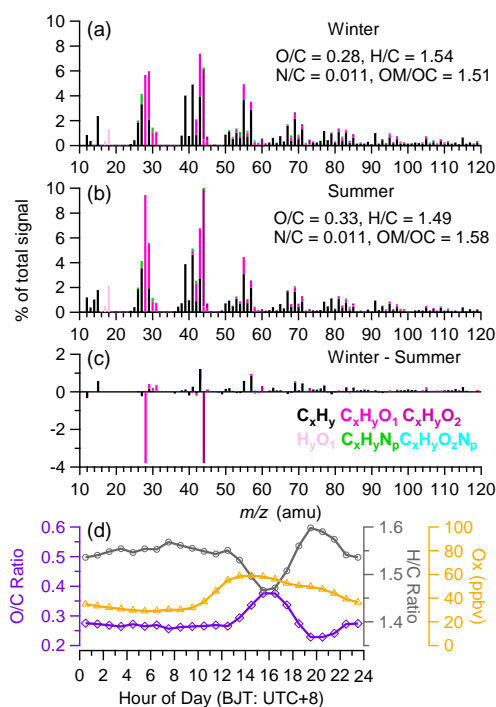
1259

1260   Fig. 6 The average HR-MS and elemental ratios of organics for (a) this study, (b) summer

1261   2012, (c) the HR-MS difference between this study and summer 2012, and (d) the

1262   diurnal variations of elemental ratios and odd oxygen ($Ox = NO_2 + O_3$).

1263

Atmospheric
Chemistry
and Physics
Discussions
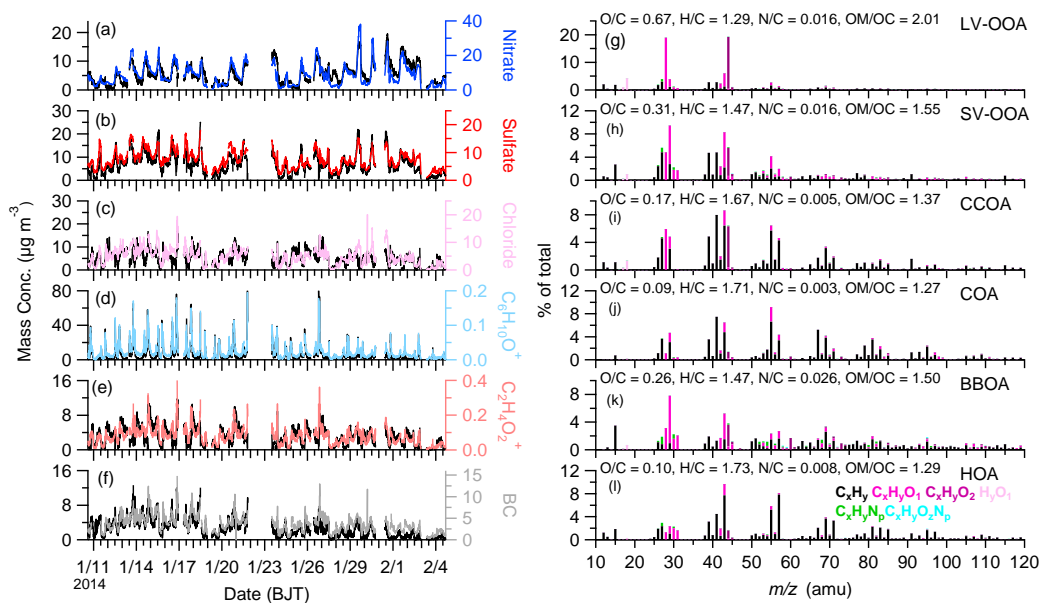
1264

Fig. 7 The PMF results of time series (a – f) and HR-MS (g – l) for each component. The

temporal variations of different tracers are also present for supporting each component.

1267
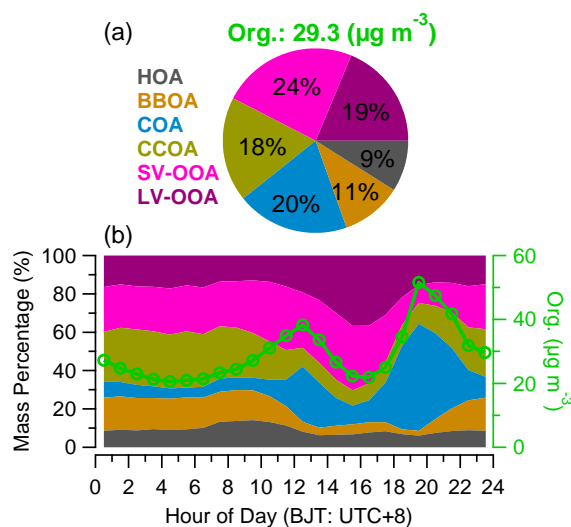
1268

Fig. 8 (a) The average mass concentration of organics and mass contributions of organic

components to organics, and (b) the diurnal variations of organic components and

organics.

Atmospheric
Chemistry
and Physics
Discussions
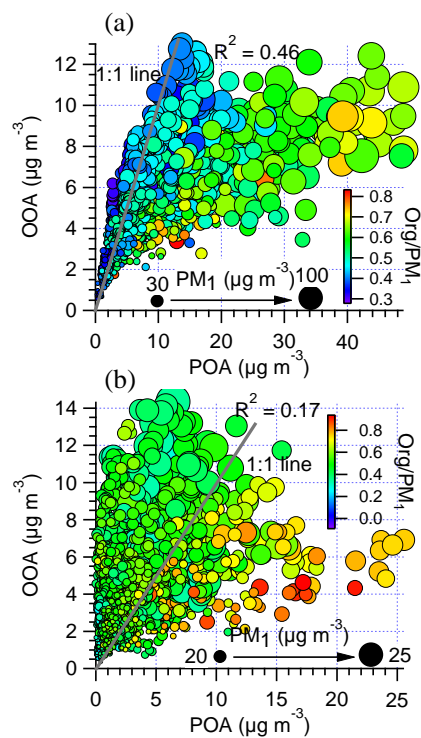
1275
Fig. 9 The scatter plot of OOA and POA colored by the ratio of Org/PM$_1$ and sized by the

1276

mass concentration of PM$_1$ for (a) winter 2013/2014 and (b) summer 2012.

1277

1278

Atmospheric
Chemistry
and Physics
Discussions
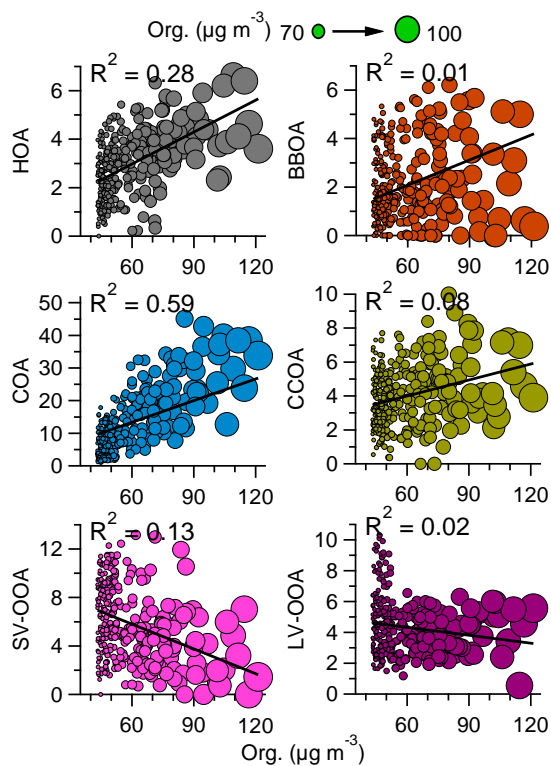
1279
1280 Fig. 10 The scatter plots of each organic component ($\mu g\ m^{-3}$) versus organics during haze

1281 periods (definite as organics > 43 $\mu g\ m^{-3}$ (Org_avg + 1σ))

1282

Atmospheric
Chemistry
and Physics
Discussions

Open Access

EGU
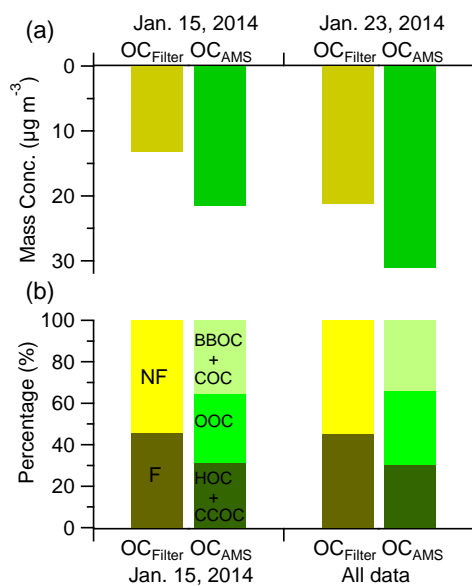
1283
1284   Fig. 11 (a) The comparisons of (a) OC concentration measured by filter sample (OC$_{Filter}$)

1285   and AMS (OC$_{AMS}$) on Jan. 15 and 23, 2014 and (b) the non-fossil (NF) and fossil (F)

1286   carbon fraction measured by ^{14}C and OC components in AMS.

1287

Atmospheric
Chemistry
and Physics
Discussions
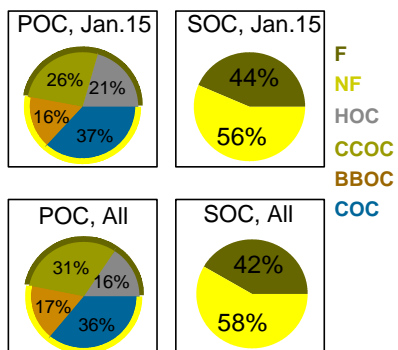
1288

1289   Fig. 12 The non-fossil (NF) and fossil (F) carbon fraction in POC and SOC during Jan.

1290   15 and all data of AMS.

1291

Atmospheric
Chemistry
and Physics
Discussions
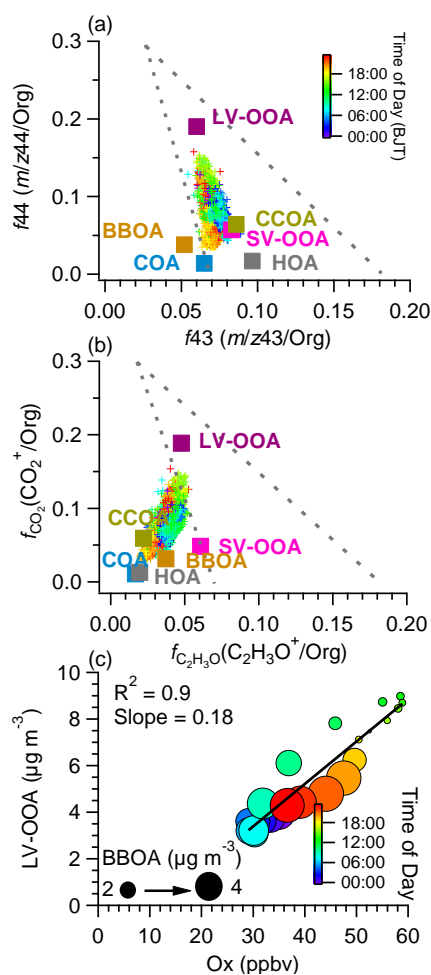
1292

1293   Fig. 13 Triangle plot of *f*44 (fraction of *m*/*z* 44 in organics) vs *f*43 (fraction of *m*/*z* 43 in

1294   organics) and (b) fCO$_2^+$ (fraction of CO$_2^+$ in organics) *vs*. fC$_2$H$_3$O$^+$ (fraction of C$_2$H$_3$O$^+$ in

1295   organics) for OA and six OA factors, and (c) scatter plot of LV-OOA *vs*. O$_x$ (the sum of

1296   O$_3$ and NO$_2$) with linear fit and colored by time of day.

1297

1298